LUND UNIVERSITY

Master of Science Thesis
VT2014

Implementation and evaluation of functional connectivity measures - a resting state fMRI study of cognitively impaired subjects

Hampus Ohlsson

Supervision

Peter Mannfolk and Olof Strandberg, Lund

Department of Medical Radiation Physics,
Clinical Sciences, Lund
Lund University
www.msf.lu.se

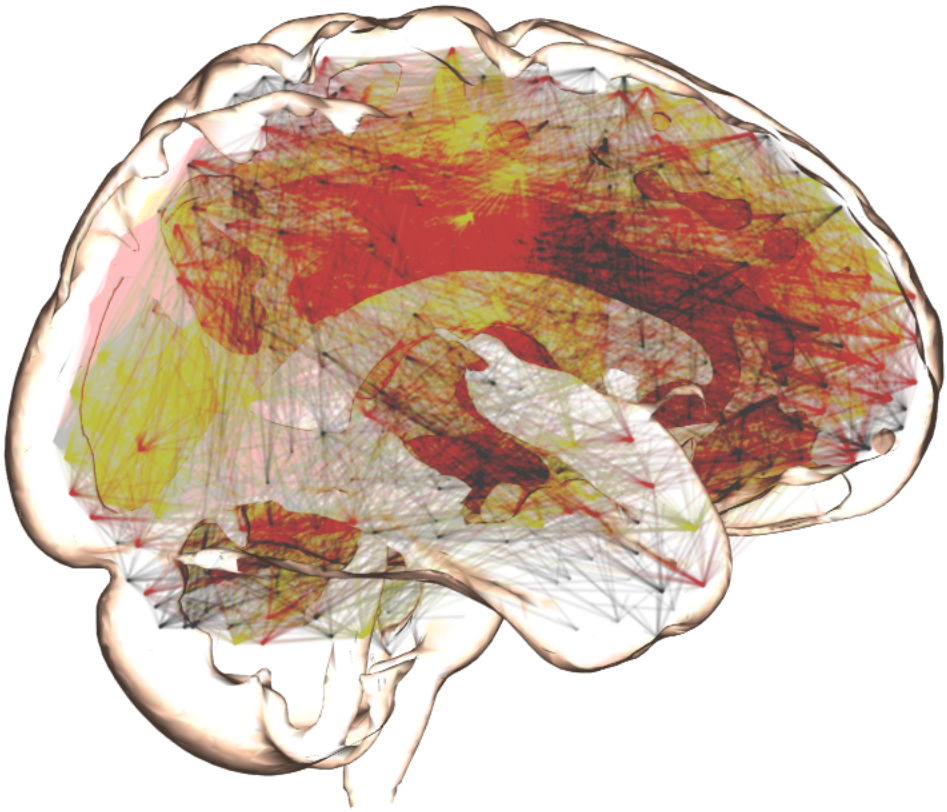

Abstract

Resting State Functional Magnetic Resonance Imaging (rs-fMRI) is often used to map brain networks or Resting State Networks (RSNs). The networks are estimated by calculating how similarly certain spatially distinct brain regions behave. These networks have been shown to differ in individuals with many different kinds of cognitive diseases.

The purpose of this study was to evaluate the capability of different network characterization measures to distinguish rs-fMRI data from subjects with Mild Cognitive Impairment (MCI) from that of healthy controls.

The measures evaluated were synchronization likelihood, mean phase coherence as well as Pearson correlation.

Four cohorts were delineated using CerebroSpinal Fluid (CSF) biomarkers and scoring in a word recollection assignment (ADAS-3). The networks of each cohort was compared to the same healthy aged matched controls.

Both synchronization likelihood and mean phase coherence was found to have lower statistical power to differentiate groups than correlation. However, the only measure capable of capturing the complex, non-linear dynamics of functional networks, synchronization likelihood, exhibits a pattern in reduced connectivity linked to perceived MCI progression.

Summary in Swedish

Funktionell magnetresonanstomografi (fMRI) är en icke-invasiv bildgivningsmetod som används för att mäta och detektera hjärnaktivitet. Tekniken utnyttjar att neural aktivering i hjärnan är kopplad till syretillförsel genom ökat blodflöde. De magnetiska egenskaperna hos blodet leder till en förhöjd radiofrekvent signal ifrån de omkringliggande vätekärnorna. När dessa radiofrekventa signaler detekteras erhålls en kontrast i de delar av hjärnan där en aktivering skett.

Traditionellt har fMRI utförts i samband med någon form av uppgift eller stimulering i syfte att upptäcka de delar av hjärnan som är kopplade till just den uppgiften eller stimulit. När så inte är fallet kallas metoden för resting state fMRI. Med resting state fMRI studeras vilka delar av hjärnan som är aktiva under vila, i frånvaro av externa stimuli.

fMRI används idag kliniskt bland annat till planering inför kirurgiska ingrepp i hjärnan för att undvika områden kopplade till viktiga funktioner såsom rörelse och tal. Studier har visat att resting state fMRI möjligen kan ersätta traditionell fMRI i detta avseende vilket hade varit fördelaktigt för patienter med svårigheter att utföra de uppgifter som krävs inom traditionell fMRI. Det har även visats att metoden kan användas till att särskilja patienter med Alzheimers sjukdom ifrån friska individer. Resting state fMRI är dock i en tidig fas av sin utveckling och fler studier är nödvändiga innan det kan användas i större utsträckning inom kliniken.

Med resting state fMRI utförs konnektivitetsanalyser mellan signalerna ifrån olika delar av hjärnan i syfte att identifiera funktionella nätverk. Tidsserier av spontan aktivitet från de olika hjärnregionerna kan jämföras med varandra för att avgöra vilka områden som är sammankopplade i ett nätverk.

I detta arbete har resting state fMRI-data från patienter med varierande grad av mild kognitiv nedsättning (MCI) jämförts med data ifrån en frisk kontrollgrupp. På så sätt kan förändringar i det funktionella nätverket i hjärnan för personer med någon form av MCI studeras.

Konnektivitetsanalysen har traditionellt utförts genom att *korrelationen* mellan olika regioner beräknats och på så sätt undersöka vilka regioner som verkar samverka med varandra och utifrån det återskapa ett funktionellt nätverk. Det finns anledning att tro att korrelation som ett mått på konnektivitet inte är det mest lämpliga i detta sammanhang.

Korrelation kan endast upptäcka lineära, stationära, samband. Det finns dock en konsensus om att hjärnan interagerar med sig själv på ett icke-lineärt sätt. Vidare, när korrelation beräknas mellan två grupper av data erhålls en koefficient med ett värde mellan -1 och 1. Negativa konnektivitetsvärden är dock olämpliga för analys av nätverkstopologi med s.k. grafteoretiska metoder.

I detta arbete implementeras två nya konnektivitetsmått samt korrelation på ovannämnda resting state fMRI-data för att utföra olika typer av nätverksanalyser. Resultaten utvärderas och analyseras utifrån dess statistiska styrka, överrensstämmelse med tidigare gjorda studier samt förmåga att detektera mönster som tyder på progression av MCI.

Det första av konnektivitetsmåtten är *synchronization likelihood*. Detta mått är avsett för att upptäcka icke-lineär, icke-stationär, synkronisation mellan två dynamiska system. I klartext betyder detta att två hjärnregioner inte behöver uppvisa identiska beteenden för att de ska anses ha ett samband utan bara att den ena regionen upprepar ett visst beteende vid två tillfällen, samtidigt som den andra regionen upprepar ett annat beteende vid samma tillfällen. Synchronization likelihood ger ett värde mellan 0 och 1 som beskriver sannolikheten att två tidsserier är synkroniserade.

Det andra konnektivitetsmåttet heter *mean phase coherence*. Detta är ett mindre allmänt mått som, precis som korrelation, endast tar hänsyn till lineära samband. Mean phase coherence kräver även att data som den implementeras på har ett oscillerande beteende. Blodflödet till hjärnans olika regioner kan dock anses bete sig någorlunda oscillerande under hjärnans vilotillstånd. Måttet infördes för att komma runt korrelationsmåttets fasskiftsberoende. I korthet kan till exempel två tidsserier med en viss fasförskjutning erhålla ett korrelationsvärde på noll trots att de för övrigt är identiska. Mean phase coherence kringgår detta genom att istället jämföra variansen i fasförskjutningen mellan två tidsserier. Detta ger ett värde mellan 0 och 1 på hur "faslåsta" två tidsserier är.

Resultaten ifrån mean phase coherence pekar på sämre statistisk styrka än de ifrån korrelation och gav begränsat med nya insikter om förändrad nätverksfunktionalitet för individer med MCI

även om vissa slutsatser angående hypotiserade progressionsmönster kan dras.

Synchronization likelihood hade också sämre statistisk styrka än korrelation men uppvisade intressanta företeelser, icke-detekterbara med korrelation, som möjligen skulle kunna ge en insikt i progressionen av MCI.

Det är därmed författarens åsikt att synchronization likelihoods lämplighet inom konnektivitetsanalys av resting state fMRI-data förtjänar fortsatta studier.

Contents

Introduction

Alzheimer's Disease (AD) is a neurodegenerative disorder affecting primarily individuals over 65 years of age with a life expectancy after diagnosis of six years[1,2]. It is the most common form of dementia and no cure exists to date. The year 2006, 26.6 million people were affected by AD[3]. The increasing age of the world's population will further increase the prevalence of the disease and by the year 2050 it is expected that one person out of 85 will be diagnosed with AD whereof 43 % will need care comparable to a nursing home[3]. The preclinical stage of AD is referred to as Mild Cognitive Impairment (MCI).

Recently, efforts to understand the mechanisms of AD have been launched as part of larger research projects namely the American BRAIN Initiative and the European Human Brain Project designed to map the human brain in its entirety down to the last neuron[4].

Today, several different modalities exist that can examine the effects of AD and MCI on the brain in a neurobiological, structural and functional way. These include measuring biomarkers in the CerebroSpinal Fluid (CSF) gathered through lumbar punctuation, positron emission tomography (PET), diffusion MRI (Magnetic Resonance Imaging) as well as electro- and magnetoencephalograms (EEG and MEG). In order to capture brain functionality with a high spatial resolution, rs-fMRI (Resting State Functional Magnetic Resonance Imaging) is the best option.

When AD has been diagnosed the window of opportunity for treatment has already past. It is therefore very desirable to discover the presence of a disease at an early stage, i.e. MCI, and understand the progression of the disease into AD. To do this, a multitude of modalities is most likely needed, each with its own strengths and weaknesses.

This report aims to compare and evaluate the suitability of certain mathematical measures in differentiating rs-fMRI data of subjects with MCI from healthy controls.

In rs-fMRI , the connectivity between different regions of the brain can be calculated[5]. These connections combine to form neural networks. The neural networks of healthy individuals differs from those of individuals with some form of cognitive impairment, for instance AD[5–9]. In order to find these networks, time series of data points representing regional oxygenation must first be measured for each brain region. These time series are referred to as Blood Oxygen Level Dependent (BOLD) time series.

The initial data contains many confounders and rigorous preprocessing is needed to find the underlying signal. After the preprocessing, the data can be used to calculate connectivity and from there, find the neural networks.

The connectivity has conventionally been measured by calculating the *correlation* between two time series originating from two corresponding brain regions. This approach is somewhat flawed due to the linear nature of the correlation operation since the way the brain interacts with itself is dynamical and highly nonlinear [10–12]. Applying a linear operation to a non-linear system will only detect the linear interdependencies. A non-linear functional connectivity measure known as '*synchronization likelihood*', as described by Stam et al. is implemented and evaluated in this report[10]. The measure takes advantage of instantaneous states in attractor space to obtain a likelihood of non-linear synchronization between two time series.

Another linear connectivity measure implemented in this report is the '*mean phase coherence*' as described by Mormann et al.[13]. Here, the variance in the instantaneous phase between two time series is examined resulting in a measurement of how 'phase locked' two time series are. Mean phase coherence was implemented mainly to test the hypothesis that progression of MCI could manifest itself as a phase shift in the interdependencies of the brain regions, a hypotheses that can not be confirmed using only correlation due to the measures dependency on the phase shift between the two time series.

With both synchronization likelihood and mean phase coherence a value between 0 (close to 0 in the case of synchronization likelihood) and 1 is obtained representing the probability of some form of connection between two brain regions. With correlation however, a value between -1 and 1 is obtained where the sign indicates the direction of their linear relationship. This becomes an issue when graph theoretical methods are applied to the data. In graph theory, the centrality designates how important a brain region is within the larger network. Some of these measures are not defined for negative values. Simply removing all non zero values or using their absolute value allows one to proceed but information is lost. What if data possessing specific interpretations are

systematically removed, changing the nature and structure of the detected network?

All three connectivity measures (synchronization likelihood, mean phase coherence and correlation) were applied to the BOLD time series of subjects to form connectivity matrices where the elements represent pairwise coupling between regions. In the graph theoretical formalism, each region is defined as a node connected by links corresponding to the pairwise couplings of the connectivity matrix. The topological properties of these graphs can then be evaluated using various measures, for example eigenvector centrality and strength.

Data from test subjects were divided into four groups based on the level of pathologically relevant CSF biomarkers in the subjects as well as their scoring in a test designed to test their cognitive function (ADAS-3). According to Hansson et al. the level of these biomarkers are indicative of the risk to develop AD in subjects with MCI[14]. Group comparisons in network connectivity between controls and each MCI group were made using permutation testing. Evaluation and analysis of the differences in the results obtained using each connectivity measure were performed. Analysis of how the neural networks seem to differ between subject groups as well as signs of progression of MCI between the groups is performed.

The group comparisons were done by first computing t-statistics of the weakening in connectivity between two brain regions for a MCI group relative controls. This was done for all unique links between two brain regions. A threshold on the t-statistic was used to remove all links not sufficiently weakened. This creates a component comprised of nodes connected by links weakened in the MCI group, i.e. a brain network with decreased functionality. The statistical significance of the network was tested using the Network Based Statistic (NBS) approach described by Zalesky et al.[15]. This approach avoids the multiple comparison problem by testing the significance of the size of the network instead of its individual links.

As a compliment to identifying a whole network with weakened connectivity, graph theoretical centrality measures can be implemented on the connectivity matrices. With these measures individual nodes, whose importance to the topological nature of the graph have changed, are identified.

Background

3.1 The BOLD signal

When a neuronal cell is activated it demands oxygen. Because of this, the neuronal activity is followed by an increase in the flow of oxygenated hemoglobin (Hb) to the cell. The amount of oxygen delivered is larger than what is needed for the activation, leading to a surplus of Hb meaning the local concentration of oxygen, cerebral blood flow (CBF) and Cerebral Blood Volume (CBV) increases in the proximity of the cell. This change of oxygenation, CBF and CBV after a neuronal activation spike is known as the hemodynamic response[16].

This hemodynamic response can be detected using fMRI. The differing magnetic properties of Hb and deoxygenated hemoglobin (dHb) serves to produce a contrast in signal strength. Hb is diamagnetic. Because the surrounding environment is also diamagnetic this will lead to increased homogeneity of the magnetic susceptibility in that environment. The increased homogeneity will lead, in turn, to an increase of the spin-spin relaxation time, T2*. dHb, on the other hand, is paramagnetic, meaning it will decrease the homogeneity causing a decrease in T2*. Thus, in a T2*-weighted image, contrast is obtained depending on the level of oxygenation. The measured signal in fMRI is thus referred to as a Blood Oxygen Level Dependent (BOLD) signal and depends on the concentration of oxygen, the CBF and the CBV. Fortunately, the relationship between this BOLD signal and the level of neural activity exhibits linear time invariant properties[17]. This means that the magnitude of the BOLD response will scale linearly with the magnitude of the neural response as well as adhere to the principles of additivity. It also means that if the neural response occurs at a certain offset in time, the BOLD response will experience the same offset.

3.2 Resting state fMRI and resting state networks

Conventional fMRI studies how the brain reacts to different forms of external input, e.g. the subject performs a series of finger tappings or is exposed to some form of visual stimuli in order to identify the regions of the brain activated under such influences. In resting state fMRI (rs-fMRI)

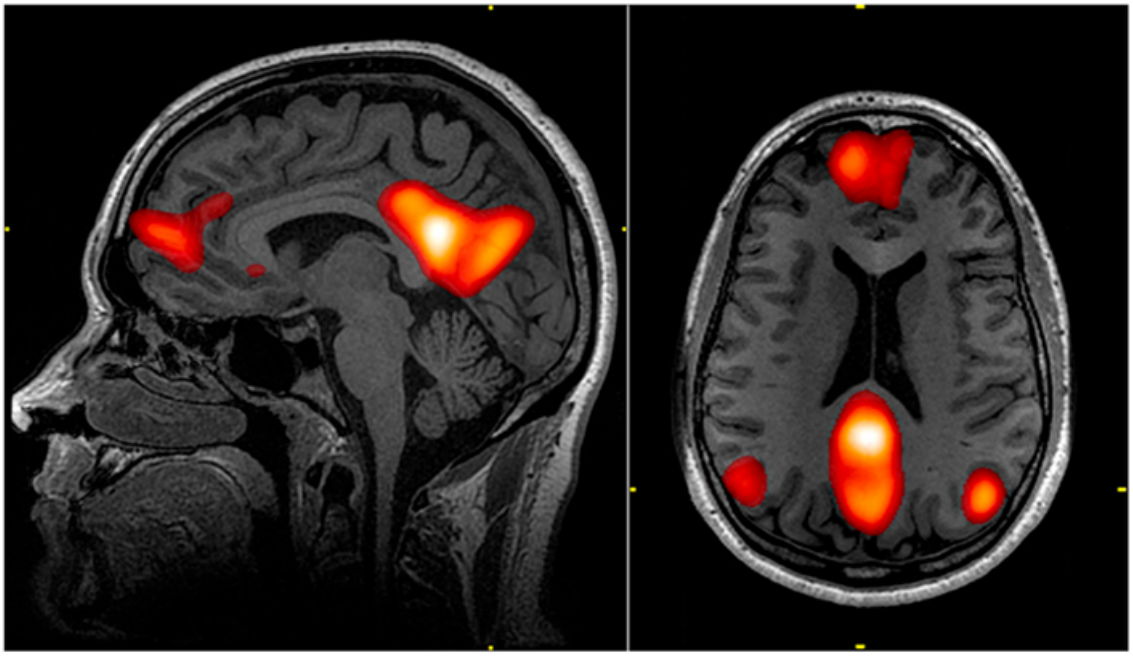

Figure 1: The default mode network, obtained through RS-fMRI. Picture obtained with permission from Graner et al.[19].

however, the subject should be isolated from all such outside influences to the largest possible degree. Simply put, the subject should be resting quietly with his/her eyes closed, i.e. in a resting state without external stimuli. By measuring spontaneous low frequency signal fluctuations in the BOLD signal it is, with rs-fMRI, possible to detect Resting State Networks (RSNs) of spatially distinct functional units within the brain[5]. The most distinct RSN that can be identified in this manner is the default mode network (DMN), see Fig. 1.

This network has been shown to increase in activity during resting state while decreasing when the subject is active[5]. The DMN is composed of mainly the medial prefrontal cortex, the posterior cingulate cortex, the inferior parietal lobule and the hippocampal formation[7, 18]. Studies imply that this network plays a role in such functions as navigating through social interactions and using past experiences to anticipate future events[18].

Other RSNs possible to detect with rs-fMRI include for instance the somatosensory, visual and auditory networks[6]. Historically, this was done using 'seed based techniques' but today it is more common to use Independent Component Analysis (ICA).

Studies have shown that AD can manifest itself as changes in the RSNs, most notably the DMN[7–9, 18]. Even subjects with other forms of dementia have been distinguished from subjects with AD using rs-fMRI[9]. It is evident that rs-fMRI is superior to conventional paradigm based fMRI in the detection and evaluation of dementia related diseases. rs-fMRI has also many advantages to other modalities. It is non invasive, contrary to lumbar punctuation of the CSF and it has a good spatial resolution contrary to PET, EEG and MEG. rs-fMRI do have a rather poor temporal resolution however (around two seconds) but several attempts to improve the temporal resolution has been made using multiband fMRI[20].

Today, RSNs are usually identified using ICA. ICA is a mathematical method that maximizes statistical independence between the BOLD time series in order to form groups (components) of functionally similar but spatially distinct ROIs[5]. Unlike the seed based technique, ICA solves the so called "blind source separation problem". This problem is often likened with a group of people talking in a room with microphones, randomly placed throughout the room, recording their conversations. With ICA it would then be possible to separate the voices of each person from each other using no other information than the recordings of the microphones[21]. The integrity of the ICA detected RSN can be tested, however, by using seed based techniques by placing the seed inside the detected RSN.

Hypotheses regarding differences in functional connectivity between corresponding subject cohorts is often analyzed using a seed based technique, in which a region in the brain is first defined as a 'seed'. The seed is then used during a rs-fMRI examination to detect voxels behaving in a similar manner to the voxels in the pre-defined brain region (hereafter referred to as a Region of Interest or ROI) using some kind of connectivity measure. The seed can be defined in different ways. One way is to take advantage of a classical stimuli-based paradigm to detect the corresponding ROI. For instance, tapping a finger during conventional fMRI and then using the activated region as a seed allows for the detection of the entire motor cortex. This was the technique first used by Biswal et al[22]. The seed can also be defined through anatomical delineation of, for instance, the hypothalamus.

It is also possible to use a multiple of ROIs, defined beforehand through some form of functional or anatomical delineation. The connectivity between every ROI to every other ROI is then computed creating a map of connectivities. If the above described seed based technique is thought of as looking at 'ROI-voxel' relationships, this technique can be thought of as looking at 'ROI-ROI' relationships. This way, each ROI works as a seed to every other ROI. This method is often used when a whole brain analysis is of interest and not just specific RSNs.

In this report, the seed-voxel connectivity analysis and ICA were not employed as we chose to adopt the whole brain ROI-ROI connectivity approach, rather than postulating hypotheses targeting specific seed regions. Furthermore, the seed-voxel connectivity analysis is computationally very demanding if implemented upon multiple ROIs.

Materials and methods

4.1 Subject group definitions and recruitment

The subject data was obtained from a study population named TiDiS (Tidig Demens i Skåne), in turn part of a larger study named Swedish BioFINDER (Biomarkers For Identifying Neurodegenerative Disorders Early and Reliably). The patients were enrolled from three different clinics in Sweden where they had been referred due to cognitive impairment. Inclusion in the study required these patients to be between 60 and 80 years of age and that their cognitive impairment did not fulfill the criteria for dementia and could not be explained by any other diagnosis. The study was approved by the Regional Ethics Comittee in Lund and all patients gave their written informed consent.

Subjects were separated into four cohorts defined by the prevalence of pathologically relevant biomarkers measured in the CSF as well as their ADAS-3 score, a part of the larger test, ADAS (Alzheimer's Disease Assessment Scale). The population size of each group will depend on which of the two motion QA:s used. All subjects were drawn from a population of totally 417 or 331 subjects (depending on the QA used).

The CSF samples were gathered through lumbar puncture of the spinal cord. The biomarkers used were β amyloid with a length of 42 amino acids (Aβ42) and phosphorylated tau (P-τ). Studies have shown that the prevalence of P-τ and the lack of Aβ42 in the CSF is indicative of AD or even the future development of AD in patients who already have MCI[14, 23]. Aβ42 is an extracellular plaque attached to neural fibres. A low prevalence of Aβ42 in the CSF is indicative of a high prevalence in the brain according to the "amyloid sink" hypothesis[23]. Simply put, a small amount of plaque in the CSF means the brain is unable to "flush out" the plaque. τ is an intracellular protein maintaining the stability of microtubule inside neurons. Oxidative stress can cause this tau protein to become hyperphosphorylated (P-τ) and be detected in the CSF [23]. P-τ is pathological because it attaches itself to healthy τ proteins causing neurofibrillary tangles. The τ proteins can not keep the microtubules from disintegrating when caught in these tangles thus leading to the death of the neuron. In summary, a low level of Aβ42 and a high level of P-τ translates to an increase in pathology.

The ADAS-3 test is a part of the larger ADAS-cog test which include several different memory related tasks where the participants are scored on each of these tasks.[24]. A larger degree of dysfunction gives a higher score. ADAS-3 focuses solely on word recollection and is inversely scored, that is the more errors a subject receives the larger her score. ADAS-3 is scored between

0-10. In this study, a score of 6-10 is therefore classified as 'objective' cognitive impairment while a score of 0-5 is classified as 'subjective' cognitive impairment. These designations arise from the subjects being perceived by themselves or relatives as having a poor or worsened cognitive ability. If this perception is not backed up by the ADAS-3 test, the subject is said to have subjective MCI, whereas if it is, the subject is said to have objective MCI.

The four MCI subject groups were named 1A, 1B, 2A and 2B. Subject group 1A, was defined as subjects with an Aβ42 level of less or equal to 647 ng/l in the CSF and classified as having subjective cognitive impairment. Depending on the motion QA used, 57 or 38 subjects were assigned to this group. Subject group 1B, was defined as subjects with a P-τ level higher than 70 ng/l in the CSF as well as being classified as being subjectively cognitively impaired. 31 or 20 subjects were assigned to this group. The same delineations were used for MCI groups 2A and 2B although these subjects were classified as objectively cognitively impaired. 58 or 52 and 29 or 24 subjects were assigned to these groups respectively. The group delineations are summarized in table 1 and visualized in Fig. 2.

It is somewhat unusual for subjects to have an Aβ42 level higher than 647 ng/l *and* a P-τ level higher than 70 ng/l. Thus, the "B-groups" largely becomes subgroups of their respective "A-group". The B-groups are more pathological than the A-groups because the B-groups are largely made up of subjects with both a low Aβ42 level and a high P-τ level. All groups are subgroups of the entire dementia population called TiDiS ('Tidig Demens i Skåne') consisting of 270 or 205 subjects in total while 147 or 126 subjects were used as age-matched healthy controls depending on the QA.

Table 1: Population sizes and defined delineations of MCI groups and control group.

	Subjects		**Aβ42**	**P-τ**	**ADAS-3**
	$FD_{mean} < 0.7$ mm	$FD_{mean} < 0.5$ mm	[ng/l]	[ng/l]	erroneous answers
Controls	147	126	-	-	-
1A	57	38	≤ 647	-	0-5 (subj. MCI)
1B	31	20	-	>70	
2A	58	52	≤ 647	-	6-10 (obj. MCI)
2B	29	24	-	>70	

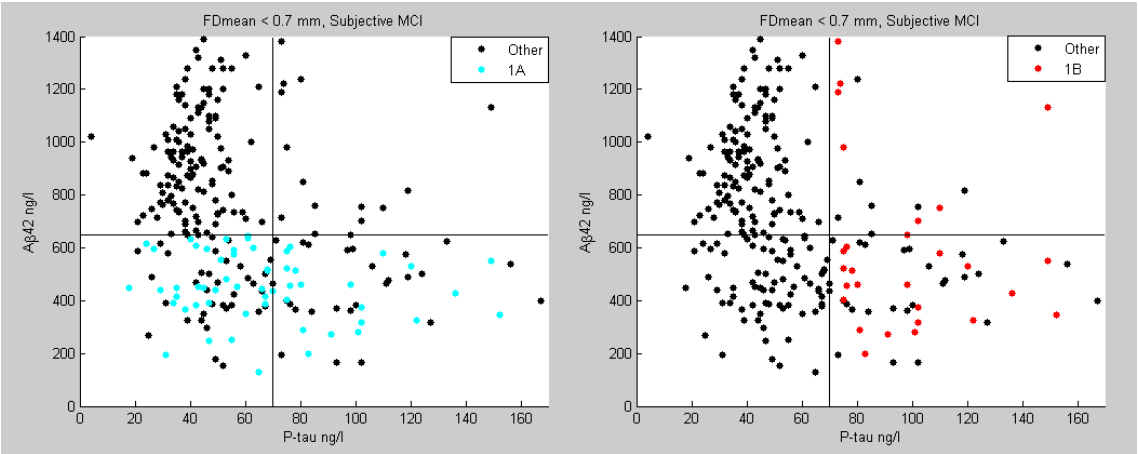

Figure 2: Biomarker distributions for 270 subjects with subjective MCI and $FD_{mean} < 0.7$mm. Cyan dots marks subjects belonging to 1A and red dots marks subjects belonging to 1B. Note that there is a large overlap between the two groups. Black dots represents subjects belonging to a group other than the ones displayed in the specific plot.

4.2 Data acquisition, pre-processing and quality assurance

A 3 T Siemens Trio scanner was used to obtain both a morphological T1-weighted volume and functional volumes for 539 subjects. The morphological volume was obtained using a fast 3D gradient echo (MP RAGE, TR=1950 ms, TE=3.4 ms) pulse sequence while a gradient echo EPI (GRE-EPI, TR=2000 ms, TE=30 ms) sequence was used for the functional volumes. The GRE-EPI pulse sequence reads the entirety of k-space during one repetition time thus minimizing the time to obtain one functional volume.

The morphological volume was obtained with a spatial resolution of 1 mm and a slice thickness of 1 mm. The functional volumes were obtained with a spatial resolution of 3.75 mm and a slice thickness of 3.75 mm. In addition, the functional volumes were smoothed with a low pass filter to a spatial resolution of 6 mm in order to reduce noise. 180 functional volumes (time frames) were obtained for each subject over a period of 6 minutes. Exclusion of the first five time frames before steady state is achieved were performed, resulting in a total of 175 time frames.

After the signal from everything except the brain was removed from the morphological volume it was transformed to fit a MNI (Montreal Neurological Institute) brain. The MNI brain is an attempt to create a 'standard' brain, representative of an average person. It was constructed by averaging the shape of 152 healthy young brains imaged with several separate scans[25]. The morphological volume was used as a 'map' for the functional volume.

A frequency band of 0.01 - 0.1 Hz was used. The upper frequency limit is used to avoid pulsating physiological noise caused by the breathing and heartbeat of the subject. The lower limit is to avoid noise caused by scanner drift. This means that interactions between the BOLD time series outside this frequency interval will be lost. This is a limitation especially concerning the higher frequencies.

To remove unwanted signal inside the frequency band, the General Linear Model (GLM) was applied. The GLM linearly determines the relative effects of n variables, $\vec{X}_{1,2,...,n}$, on the observed signal $\vec{Y}$[17]. In this case, $\vec{Y}$ is the magnitude of the BOLD time series signal in each voxel of the functional volume whereas $\vec{X}_{1,2,...,n}$ are noise parameters, referred to as a nuisance regressors. The GLM can be expressed as:

$$\vec{Y} = \beta_0 + \beta_1\vec{X}_1 + \beta_2\vec{X}_2 + ... + \beta_n\vec{X}_n, \tag{1}$$

where $\beta_1, \beta_2, ..., \beta_n$ denotes the contribution of each nuisance regressor and β_0 describes where the function crosses the Y-axis. 34 nuisance regressors were implemented in the GLM. To correct for motion, 12 regressors representing each of the six degrees of freedom (three translational degrees and three rotational degrees) at two consecutive time points were used. The square of each of these regressors were also implemented to increase the sensitivity of the motion correction[26]. This amounts to a total of 24 regressors concerning motion artifacts.

Two of the remaining regressors deals with signal originating in white matter and the CSF but positioned in voxels defined as gray matter. This signal is not of interest since all neural activity occurs in gray matter. This unwanted signal is dealt with by first delineating the white matter and CSF and then averaging the time series of all constituent voxels. The averaged time series are then used as nuisance regressors in each gray matter voxel.

During the course of the project it became evident that the above described motion correction alone was not satisfactory. Therefore, an additional outlier correction were introduced using the "global signal". The global signal is the sum of all voxels at a certain time point. If the global signal varies a lot for a specific volume it is quite likely due to motion of the subject's head. If this is the case, an additional regressor is added to the GLM of that volume.

This outlier correction involved the use of time frames classified as having an outlying signal relative a reference volume, using the FSL motion outlier tool. If the root mean square of the global signal differs between a given volume and a reference volume above a certain threshold, that time frame is considered an outlier and added to the GLM as a regressor for all other time frames. Since we now model the offending time point in the GLM, its influence is removed from the estimation of all effects of interest.

Furthermore, even though the use of a frequency band does away with most of the physiological noise, some will remain. These pulsating effects may be dealt with using a principal component analysis based method called CompCorr as described by Bezhadi et al.[27]. This method takes

advantage of certain anatomical areas known for their pulsating behavior to form noise ROIs. Six of these noise ROIs are formed, the time series of their voxels averaged and used as regressors in all gray matter voxels. The two remaining regressors were used to deal with the linear drift in the measured signal due to heating of the gradient coils as well as a separate quadratic drift in the measured signal(possibly caused by gradual motion).

Additional pre-processing outside the GLM included a slice timing correction. Slice timing correction is used to avoid effects caused by the signal from different slices in the volume being read at different points in time. Since the entirety of the volume is read during one repetition time with an EPI pulse sequence the time difference between two slices may be up to 2 seconds in this case. To align the slices in time, a reference slice is chosen where after each slice is interpolated to match that slice.

To correct for bulk motion, that is rough movement of the entirety of the skull, each functional volume in a certain time frame is linearly transformed to fit it's neighboring volume starting from the middlemost volume.

4.2.1 The FD based QA

Sometimes data is so distorted by motion it can not be saved using any correction techniques. If this is the case, the data must be discarded using a Quality Assurance (QA). The QA implemented on the data in this report uses the concept of Framewise Displacement (FD) as described by Power et al.[28]. Instead of simply removing subjects with a translational or rotational movement in any direction above a certain threshold between two, in time, neighboring volumes, the FD is a measure that takes into account all the six degrees of freedom at once. The FD for a time frame, i, is the combined displacement in all six degrees of freedom compared to a neighboring time frame:

$$FD_i = |\Delta d_{ix}| + |\Delta d_{iy}| + |\Delta d_{iz}| + |\Delta \alpha_i| + |\Delta \beta_i| + |\Delta \gamma_i| \tag{2}$$

where x, y, z are the translational directions and α, β, γ are the rotational directions. Power et al. converted the rotational displacements from degrees to mm by approximating the brain as a sphere with a radius of 50 mm and calculated the displacement on the surface of this sphere caused by a rotational displacement[28]. For instance, a rotational displacement of 1 degree results in a converted displacement of 0.87 mm.

The FD between two neighboring volumes was calculated and averaged over the whole examination:

$$FD_{mean} = \frac{1}{175} \sum_{i=1}^{175} FD_i \tag{3}$$

Two different thresholds on the FD_{mean} were used. Subjects with a FD_{mean} above 0.5 mm or above 0.7 mm were removed. Note that all results presented are characterized as belonging to one of these FD_{mean} defined QA groups.

4.3 ROI definition

Although it is possible and sometimes of interest to make a voxelwise comparison of all the time series, it is computationally extremely demanding. Instead, the voxels were grouped together into ROIs and the constituent voxel time series of these ROIs were averaged into one time series for each ROI.

The ROIs were defined as functionally and spatially coherent regions through a spatially constrained spectral clustering approach as described by Craddock et al.[29]. What this clustering approach does is to give each pair of neighboring voxels a weighted connection depending on the similarity of their respective time series. Then, through iterative methods, weaker connections are broken until a pre-determined number of clusters (ROIs) are obtained. This method ensures that the similarity between the time series of voxels within a ROI are maximized compared to the time series of voxels between ROIs, thus forming a pre-determined number of functional units. 840 functionally distinct ROIs were used. This was the largest set of pregenerated ROIs using functional parcellation provided by Craddock et al. These ROIs will have an overlap with one or more of the anatomical volumes defined in the Automated Anatomical Labeling (AAL) brain

atlas[30]. The AAL brain atlas consists of 90 anatomical units. The defined ROIs can be seen in Fig. 3.

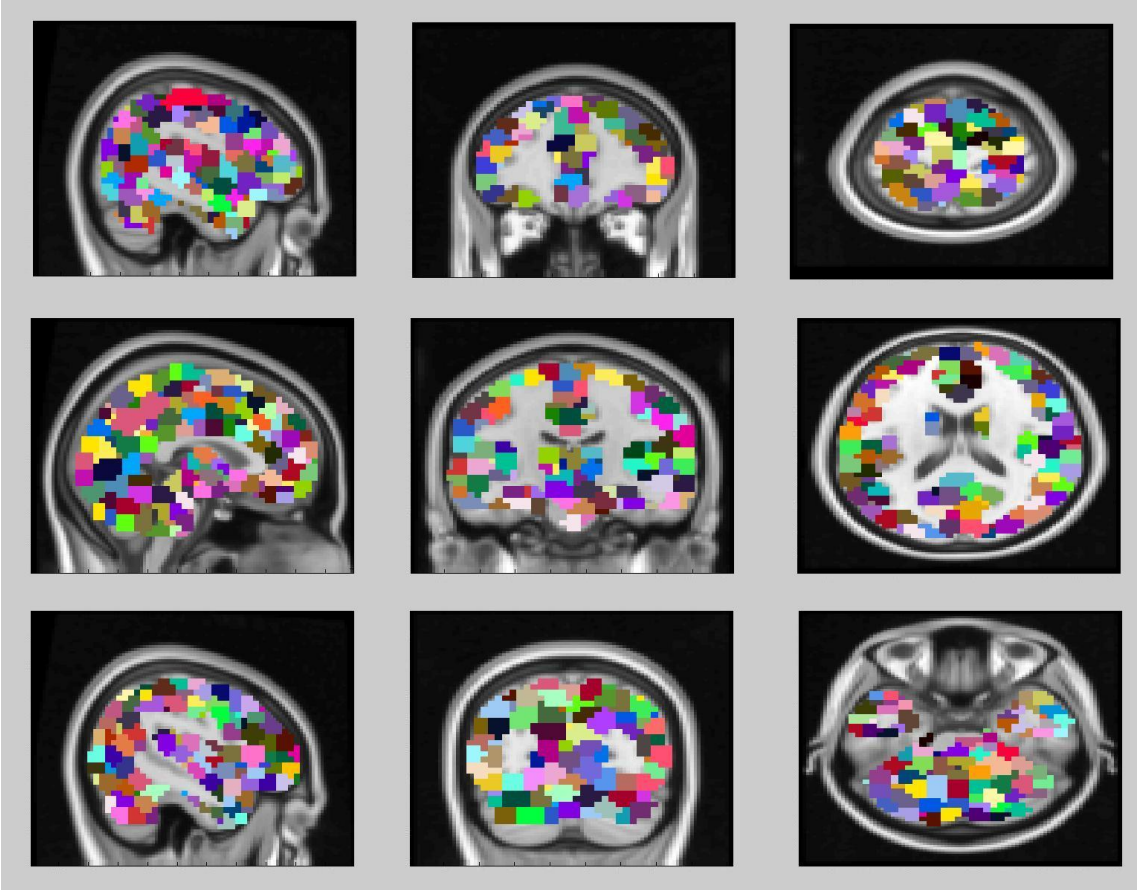

Figure 3: Defined ROIs in the sagittal, coronal and axial plane displayed with arbitrary colors. In total, 840 ROIs were defined.

4.4 Calculations

From the original time series, connectivity matrices were computed using correlation, mean phase coherence and synchronization likelihood. For a detailed description of synchronization likelihood and mean phase coherence see Secs. 4.4.2 and 4.4.3 respectively. These matrices were computed for each subject and displays the connectivity between each of the 840 ROIs shown in Fig. 3. Three connectivity matrices of the same subject obtained with each of the three methods are shown in Fig. 4. The axis denote the brain region and the color scheme reflects the level of connectivity. Note that the diagonal halves are reflections of each other since only symmetrical connectivities are considered in this report. Note also the partly negative scale in the correlation matrix. Elements along the main diagonal are zero because self connections are not considered.

All computations were done in MATLAB version 7.12.0 unless otherwise stated.

4.4.1 Graph theory

The above mentioned connectivity matrices can be seen as graphs according to graph theory. A graph in this context is a mathematical structure consisting of nodes (sometimes referred to as vertices) connected by links (sometimes referred to as edges). In this case the nodes represents the 840 ROIs previously defined while the links represents an element in one of the connectivity matrices (Figs. 4 and 10) i.e. the level of connectivity between two nodes. The graphs are undirected meaning the links do not point in any direction (the elements in the connectivity matrices are scalars).

A graph, G may be defined as

$$G = (V, E) \tag{4}$$

where $V = (v_1, v_2, ...v_n)$ describes the nodes in the graph and $E = (e_1, e_2, ..., e_{\frac{n\times(n-1)}{2}})$ describes each unique link between each of the nodes[31]. As stated before, this graph can be represented as a connectivity matrix. This connectivity matrix can either be weighted as in Fig. 4 or binary as in Fig. 10. In the following sections, different ways of calculating the value of each node-node link are described i.e. synchronization likelihood and mean phase coherence.

4.4.2 Synchronization likelihood

One of the issues with correlation as a connectivity measure is that it can only detect linear and symmetric interdependencies between the BOLD time series of the different nodes[11]. The interactions of the functional components within the brain is far from linear however. The data within the time series behave in a non-stationary manner and the dynamical interdependencies between the different time series may change rapidly[10]. The concept of synchronization likelihood have previously been implemented with success in studies primarily involving electroencephalograms and magnetoencephalograms[10, 11] (EEGs and MEGs) but also in studies involving fMRI[32]. Synchronization likelihood is based on the concept of generalized synchronization as described by Rulkov et al.[33]).

Two interacting chaotic systems (in this case, each time series may be thought of as a system) may be synchronized with each other. This synchronization may not only take the form of equality between individual variables in the different systems however. Generalized synchronization exists between two systems, X and Y, when the state of the response system, Y, is a function of the state of the driver system, X:

$$Y = F(X). \tag{5}$$

Taken's theorem describes how an attractor can be represented from a series of measured data points, i.e. the BOLD time series, using so called 'time embedding', preserving topological properties of the dynamical system[34]. This means that the time series contain information about the non linear dynamical system (the brain). In this case, two time series represents an attractor with an associated, unknown and non-linear differential equation depending on a number of parameters and a noise variable. Provided Eq. (5) is true and F is continuous it follows that if two states of X, x_i and x_j, are very close together in attractor space (or state space), then the corresponding points of Y, y_i and y_j, are also very close together[10]. By measuring the connectivity between two time series in this manner, the series may look completely different from each other and still have a high synchronization likelihood, providing one of them keeps displaying a certain behavior at the same time as the other displays another behavior, see Fig. 5. Synchronization likelihood takes advantage of this in order to calculate an index reflecting the likelihood that two time series are non-linearly synchronized with each other.

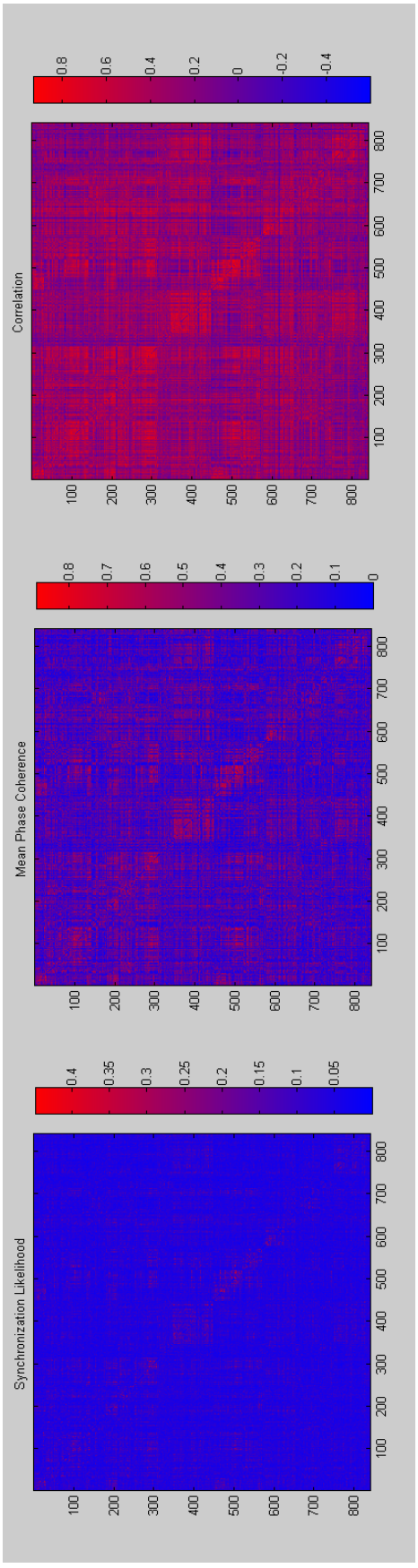

Figure 4: Connectivity matrices, or graphs, representing the level of connectivity between each of the 840 nodes. Computed with synchronization likelihood, mean phase coherence and correlation.

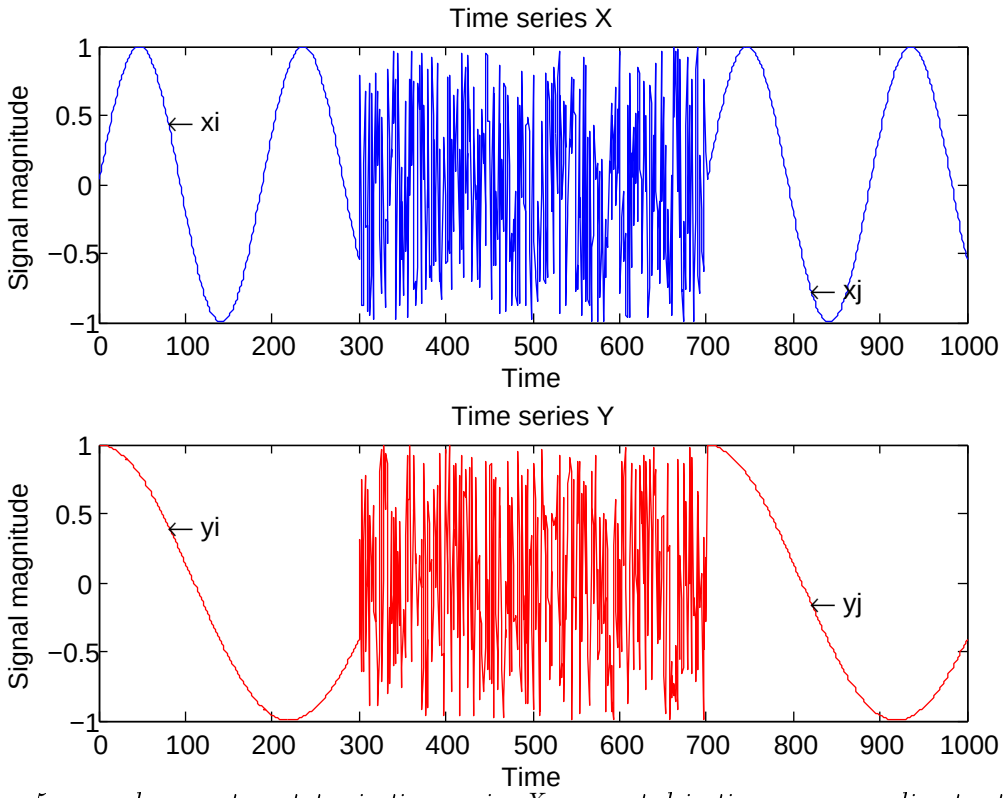

Figure 5: x_i and x_j are two states in time series X, separated in time, corresponding to states y_i and y_j in time series Y. Although the two time series behaves differently to one another they both display a recurring behavior at the same points in time and are therefore synchronized.

Consider M recorded time series, $\vec{x}_{k,} = x_{k,1}, x_{k,2}, ..., x_{k,N}$, where $k = 1, 2, ..., M$ denotes the node and N the number of sampled data points. From each of these M time series $N - m + 1$ time embedded vectors, $\vec{X}_{k,i}$, are constructed:

$$\vec{X}_{k,i} = x_{k,i}, x_{k,i+1}, x_{k,i+2}, ..., x_{k,i+m-1} \tag{6}$$

where m is the number of elements in each time series embedded vector (referred to as the time embedding dimension) and N is the number of discrete time points in a time series. According to chaos theory, the correlation integral, C_k, is the mean probability that two different states in the same system are closer to each other in attractor space than a certain distance, ε_k:

$$C_k(\varepsilon_k) = \lim_{N\to\infty} \frac{1}{N^2} \sum_{\substack{i,j=1 \\ i\neq j}}^{N} \Theta(\varepsilon_k - |\vec{X}_{k,i} - \vec{X}_{k,j}|) \qquad ; \vec{X}_{k,i,j} \epsilon \mathbb{R}^m. \tag{7}$$

The distance, $|\vec{X}_{k,i} - \vec{X}_{k,j}|$, may refer to the Euclidean distance, the city block distance, the correlation distance (one minus the correlation between the two vectors) or any other kind of distance measurement. Θ is the Heaviside step function, defined as $\Theta(x) = 0$ if $x \leq 0$ and $\Theta(x) = 1$ if $x \geq 0$.

The correlation integral in Eq. (7) can be estimated as a discrete sum called the correlation sum:

$$C_k(\varepsilon_k) = \frac{1}{N(N-1)} \sum_{\substack{i,j=1 \\ i\neq j}}^{N} \Theta(\varepsilon_k - |\vec{X}_{k,i} - \vec{X}_{k,j}|). \tag{8}$$

Eq. (8) computes the distance between every pair of time embedded vectors except when $i = j$. To avoid calculating a distance twice (for example calculating $|\vec{X}_{2,1} - \vec{X}_{1,2}|$ when $|\vec{X}_{1,2} - \vec{X}_{2,1}|$ has

already been calculated) Eq. (8) may be modified to only take into account unique pairs:

$$C_k(\varepsilon_k) = \frac{1}{N(N-1)/2} \sum_{\substack{i,j=1 \\ i \neq j}}^{N} \Theta(j-i+1)\Theta(\varepsilon_k - |\vec{X}_{k,i} - \vec{X}_{k,j}|). \tag{9}$$

To avoid the issue of autocorrelation, that is, when the distance between $\vec{X}_{k,i}$ and $\vec{X}_{k,j}$ is smaller than ε_k only because their time overlap is large, Theiler's correction for autocorrelation, w, is introduced. w describes how much $\vec{X}_{k,i}$ and $\vec{X}_{k,j}$ overlaps. Say $w = 2$, this means that if $i = 1$, $j = 2$ and $m = 5$ then $\vec{X}_{k,i} = x_{k,1}+x_{k,2}+x_{k,3}+x_{k,4}+x_{k,5}$ and $\vec{X}_{k,j} = x_{k,3}+x_{k,4}+x_{k,5}+x_{k,6}+x_{k,7}$. Equation (9) represents the special case of $w = 1$. An arbitrary w gives:

$$C_k(\varepsilon_k) = \frac{1}{(N-w)(N-w+1)/2} \sum_{\substack{i,j=1 \\ i \neq j}}^{N} \Theta(j-i-w+1)\Theta(\varepsilon_k - |\vec{X}_{k,i} - \vec{X}_{k,j}|). \tag{10}$$

A constant, p_{ref}, is now introduced. p_{ref} describes the fraction of time embedded vectors ,in a time series, close enough to the reference time embedded vector, $\vec{X}_{k,i}$, for them to be considered occupying the same state. Here, we set $p_{ref} = 0.05$ meaning 5 % of all vectors within a time series will be considered recurrences of $\vec{X}_{k,i}$. This applies for all vectors, that is, for all $\vec{X}_{k,i}$. This introduces a critical distance, $\varepsilon_{k,i}$, which is decided by p_{ref}. For each $\vec{X}_{k,i}$, there exists a critical value of $\varepsilon_{k,i}$ that fulfills the condition set by p_{ref}, the condition that 5 % of all other vectors in that time series should be occupying the same space. Optimally, we seek to satisfy p_{ref}=$C_k(\varepsilon_k)$. Since there is only one C_k for each time series, $\varepsilon_{k,i}$ for all discrete time points is averaged into the aforementioned ε_k. This is done by finding an optimal value of ε_k so that the criteria defined by p_{ref} is true for as many time embedded vectors as possible.

For each node's time series, an optimal value of ε_k is calculated through convergence of $C_k(\varepsilon_k) \rightarrow p_{ref}$. In other words, ε_k is varied to find the value of $C_k(\varepsilon_k)$ closest to p_{ref} thus giving the optimal ε_k. For an illustrative example, see Fig. 6.

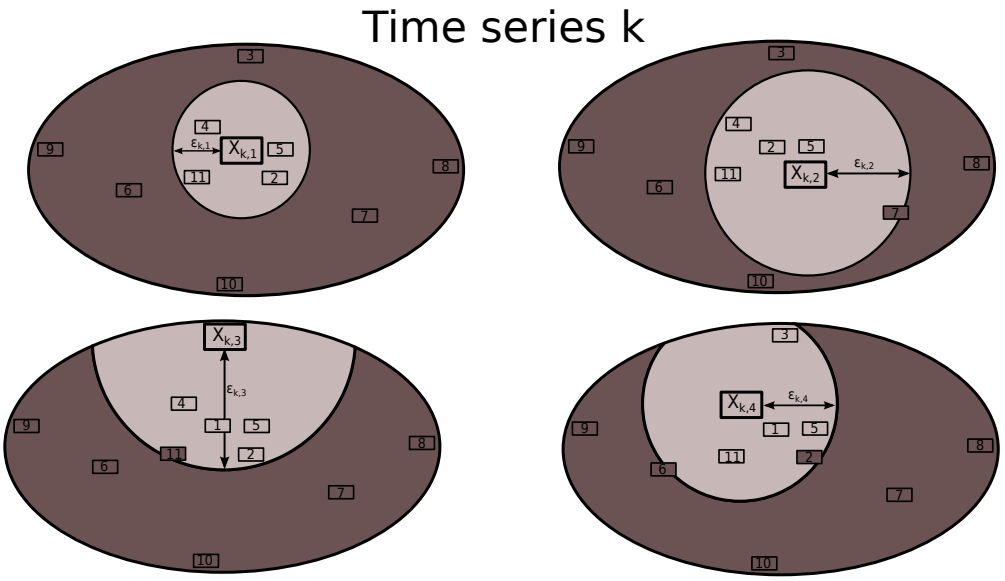

Figure 6: Illustration of ε_k in state space. For each time embedded vector, $X_{k,i}$, in time series k, a critical distance, $\varepsilon_{k,i}$, is calculated that satisfies the predefined condition set by p_{ref}. This is done through convergence of the correlation integral to p_{ref}. To obtain one value for $C(\varepsilon_k)$, the critical distances are averaged into ε_k meaning the criteria set by p_{ref} will not necessarily be true for all time embedded vectors. This example shows $i = 1, 2, 3, 4$ for totally 11 time embedded vectors in state space each with their own $\varepsilon_{k,i}$. $p_{ref} = 4/10$, meaning four out of ten states are considered recurrences of the reference state.

Now, with an optimal ε_k calculated for each time series, the synchronization likelihood, S, between two nodes, k and l, is given by:

$$S_{k,l} = \frac{1}{p_{ref}} \frac{1}{(N-w)(N-w+1)/2} \sum_{\substack{i,j=1 \\ i \neq j}}^{N} \Theta(j-i-w+1)\Theta(\varepsilon_k - |\vec{X}_{k,i} - \vec{X}_{k,j}|)\Theta(\varepsilon_l - |\vec{X}_{l,i} - \vec{X}_{l,j}|). \tag{11}$$

This is done for each unique combination of two separate nodes. If there are N_R nodes, then $\frac{N_R(N_R-1)}{2}$ S-values will be calculated.

Eq. (11) describes how likely it is that a synchronization exists between the time series of node k and node l normalized with p_{ref} to achieve a value between p_{ref} and 1. $S_{k,l}$ can also be described as the likelihood of a recurring state in time series k at a time point i being associated with a recurring state in time series l averaged across all discrete time points, i. For an illustrative example, see Fig. 7.

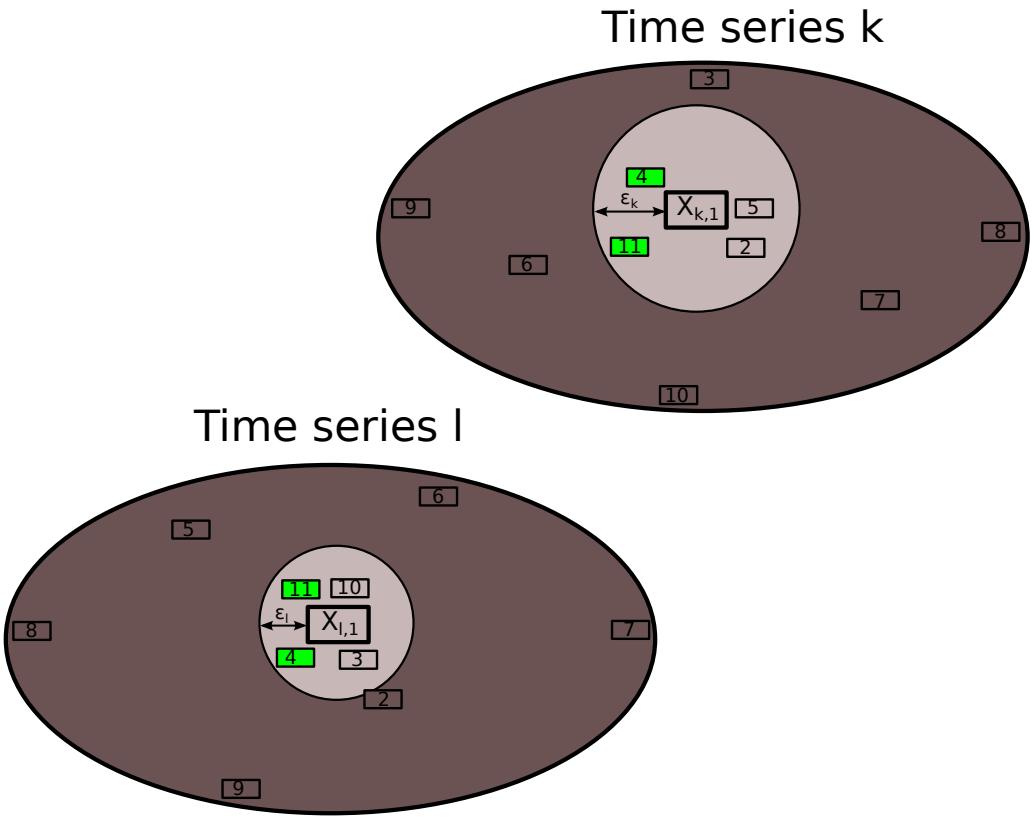

Figure 7: Illustration of the synchronization likelihood index in state space where $p_{ref} = \frac{4}{10}$. In time series k at the discrete time point $i = 1$ the time embedded vectors at the discrete time points $j = 2, 4, 5, 11$ are considered recurrences of the reference time embedded vector, $X_{k,1}$. Correspondingly, the time embedded vectors at the discrete time points $j = 3, 4, 10, 11$ are considered recurrences of reference time embedded vector, $X_{l,1}$ in time series l. Two of these states ($j = 4, 11$) are considered recurrences in both *time series. At the discrete time point of $i = 1$ the synchronization likelihood is thus $S = 2/10$ since two out of ten possibles states are simultaneous recurrences. To obtain the synchronization likelihood across the whole length of the time series the procedure has to be repeated for $i = 1, 2, ..., 11$ and the result averaged.*

Note that it is not possible to discern which region is the driver system and which is the response system using this method i.e. the graph is undirected.

The time embedding dimension, m, and Theiler's correction for autocorrelation, w, was both set at a value of 9 to avoid any overlap. p_{ref} was set at 0.05. The distance measure between time

embedded vectors was chosen to be the correlation distance. Results with very weak statistical power were obtained using $m = 20$, the Euclidean distance measure or the city block distance measure and are therefore not reported on further.

Weighted Synchronization likelihood In the approach described above, all distances between two time embedded vectors lower than a cut off value obtains the same weight (Eq. (10)). In order to put more emphasis on shorter distances, a weighting element can be implemented in the function. Eq. (10) can be rewritten as:

$$C_k(\varepsilon_k) = \frac{1}{\sum_{i,j=1}^{N} \Theta(j-i-w+1)\frac{1}{|\vec{X}_{k,i}-\vec{X}_{k,j}|+\gamma}} \sum_{i,j=1}^{N} \Theta(j-i-w+1)\frac{\Theta(\varepsilon_k - |\vec{X}_{k,i}-\vec{X}_{k,j}|)}{|\vec{X}_{k,j}-\vec{X}_{k,j}|+\gamma} \quad (12)$$

where γ is an arbitrary factor in this case set to 1 in order to avoid instability when $|\vec{X}_{k,j} - \vec{X}_{k,j}| \to 0$.

By extension, the final synchronization likelihood formula, Eq. (11)), is modified into:

$$S_{k,l} = \frac{1}{p_{ref}} NF_{l,k} \sum_{i,j=1}^{N} \Theta(j-i-w+1)\frac{\Theta(\varepsilon_k - |\vec{X}_{k,i}-\vec{X}_{k,j}|)}{|\vec{X}_{k,i}-\vec{X}_{k,j}|+\gamma}\frac{\Theta(\varepsilon_l - |\vec{X}_{l,i}-\vec{X}_{l,j}|)}{|\vec{X}_{l,i}-\vec{X}_{l,j}|+\gamma}. \quad (13)$$

where the entire second factor is a normalization factor, thus Eq. 13 is rewritten as:

$$S_{k,l} = \frac{1}{p_{ref}} \frac{1}{\sum_{i,j=1}^{N} \Theta(j-i-w+1)\frac{1}{|\vec{X}_{k,i}-\vec{X}_{k,j}|+\gamma}\frac{1}{|\vec{X}_{l,i}-\vec{X}_{l,j}|+\gamma}} \sum_{i,j=1}^{N} \Theta(j-i-w+1)\frac{\Theta(\varepsilon_k - |\vec{X}_{k,i}-\vec{X}_{k,j}|)}{|\vec{X}_{k,i}-\vec{X}_{k,j}|+\gamma}\frac{\Theta(\varepsilon_l - |\vec{X}_{l,i}-\vec{X}_{l,j}|)}{|\vec{X}_{l,i}-\vec{X}_{l,j}|+\gamma}. \quad (14)$$

The distances between all time embedded vectors are now weighted between 1/3 and 1, provided the distance is lower than ε_k where short distances gain higher weights. The idea is that more focus will be placed on the most essential connections in the network.

Very weak results were obtained using the weighted synchronization likelihood however and are therefore not reported on any further.

4.4.3 Mean phase coherence

A somewhat less general connectivity measure is the mean phase coherence as described by Mormann et al.[13] and Rosenblum et al.[35]. This method uses the mean phase coherence as a measure of phase synchronization between two systems. Similar to synchronization likelihood, the method has mostly been implemented in studies involving EEG and MEG[13]. In contrast to synchronization likelihood however, this method assumes the time series in question behave in an approximately oscillatory fashion and can only detect linear interactions[10, 13].

This measure was implemented to test a hypothesis that progression of the MCI expresses itself as a gradual phase shift of the interdependencies between certain nodes. Progression of MCI is here hypothesized to be expressed as a decrease in the Aβ42 and an increase in the P-τ as well as a lowering of the ADAS-3 score. So according to this hypothesis, a decrease in the Aβ42 and the ADAS-3 score as well as an increase in the P-τ leads to a larger phase shift between the BOLD time series of certain nodes. In practice, this simple hypothesis of the progression of MCI means a transfer from group 1A to 1B, 2A and finally 2B.

The correlation between two oscillating functions is dependent on the phase shift between them. For instance, if two identical oscillating functions are phase shifted in regards to each other by $\pi/2$ radians there will be no correlation between them, see Fig. 8. Using correlation, it is not possible to say whether there is no correlation between two nodes because there is no interaction between them or simply because the phase shift between their respective time series happen to fall within an unfortunate interval.

This phase shift dependency can also affect the group comparisons. Assume there exists some 'natural' phase shift between two nodes, that is, the phase shift the controls would be expected to have. If correlation is used, the contrast between controls and MCI group will then not only be caused by a weakening between the brain regions in question but also the difference in the phase shifts between the subject groups. Fig. 9 illustrates how correlation, and thus the contrast between groups, can depend on the phase shift.

Mean phase coherence, on the other hand, is independent of phase shift. When using mean phase coherence, a contrast in network connectivity will depend solely on an actual weakening of connectivity between nodes.

Thus, if a contrast is obtained using mean phase coherence but not with correlation that contrast should come from a weakening of connectivity not related to an increased phase lag. Vice versa, if a contrast is obtained with correlation but not with mean phase coherence it should be because of a phase shift.

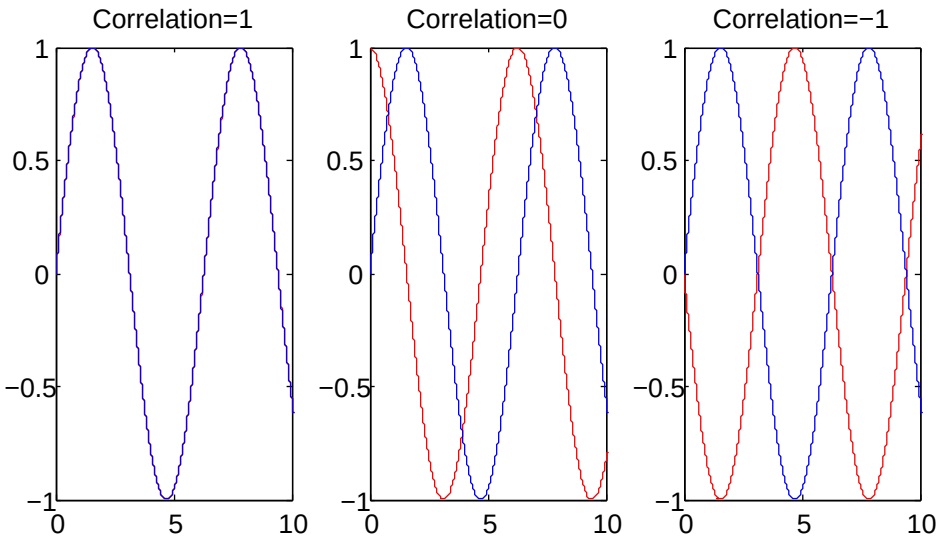

Figure 8: Two identical time series phase shifted (from left to right) 0, $\pi/2$ and π radians. Although the two time series display very similar behavior in all three cases there exists no correlation with a phase shift of $\pi/2$ radians. Also, the negative correlation is not usable when different kinds of measures concerning graph topology are implemented. Using mean phase coherence, the two time series are identified as having a perfect phase locking in all three cases.

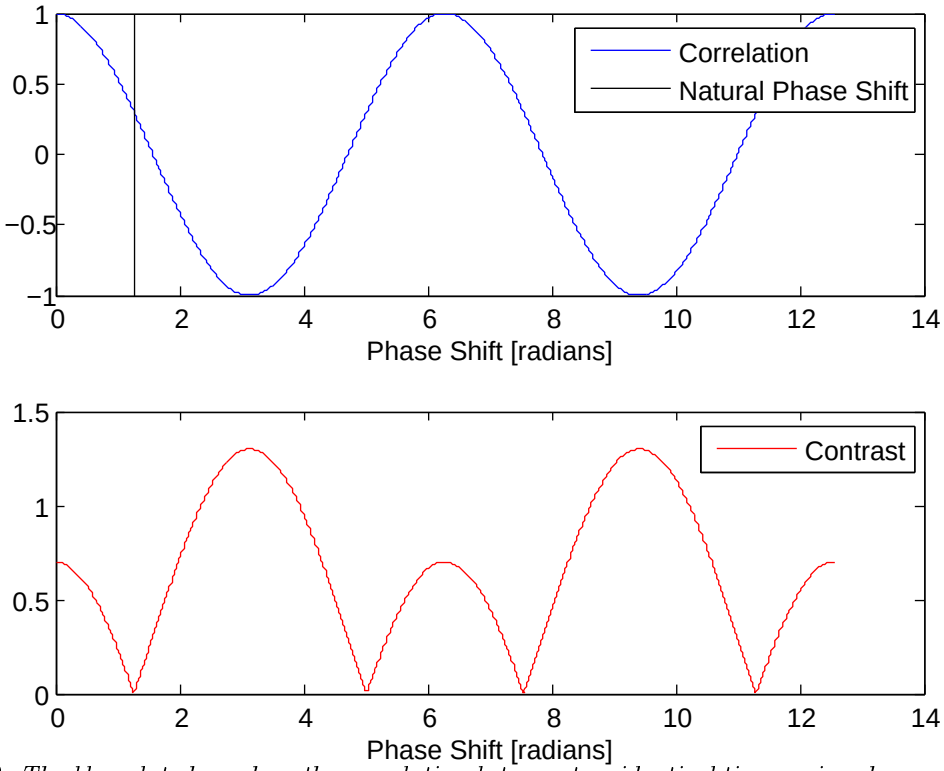

Figure 9: The blue plot shows how the correlation between two identical time series changes depending on their phase shift. The black bar indicates the phase shift of the control group. The natural phase shift and thus the level of the black bar was chosen arbitrarily for explanatory purposes. The red plot shows how the contrast between the MCI group and control group will vary with the phase shift in the MCI group assuming the same natural phase shift as before. Note that the contrast when using mean phase coherence will be a flat line (positioned at 0 if the time series are identical).

In the classical sense, phase synchronization is defined as locking of the phases of two oscillators:

$$\varphi_{n,m}(t) = n\phi_a(t) - m\phi_b(t) = constant \tag{15}$$

where n and m are integers, ϕ_a and ϕ_b are the phases of each oscillator and $\varphi_{n,m}$ is referred to as the relative phase. Following the analytical signal approach, the instantaneous phase, $\phi(t)$ of a time series, $x(t)$, is given by

$$\phi(t) = \arctan\left(\frac{\tilde{x}(t)}{x(t)}\right) \tag{16}$$

where

$$\tilde{x}(t) = \mathrm{Im}\left(\frac{1}{\pi} p.v. \int_{-\infty}^{\infty} \frac{x(\tau)}{t-\tau} d\tau\right) \tag{17}$$

which is the imaginary part of the Hilbert transform of $x(t)$. $p.v.$ denotes the Cauchy principle value. Given, $\phi(t)$, for two time series, $x(t)$ and $y(t)$, assumed to behave oscillatory, Eq. (15) gives

$$\varphi_{1,1}(t) = \phi_x(t) - \phi_y(t) \tag{18}$$

where $n = m = 1$ because, according to Mormann et al., it is most likely to detect phase synchronization at a phase locking ratio of 1:1. The reasoning behind this is that all the time series are part of the same physiological system (i.e. the brain)[13]. Therefore, it is deemed more likely that the time series oscillate with the same frequency than that they oscillate with multiples of each others frequencies.

In order to achieve a connectivity measure between two nodes, the mean phase coherence, R, is defined as

$$R = \left|\frac{1}{N}\sum_{t=1}^{N} e^{i\varphi_{1,1}(t)}\right| = 1 - CV \tag{19}$$

where CV is the circular variance, i.e. the angular variance of $\varphi_{1,1}$ transformed to the unit circle in the complex plane. CV is therefore a measure of how much the relative phase between two time series differs averaged across a certain period of time. Mean phase coherence is thus not dependent on the actual phase shift but instead the *variance* in the phase shift.

4.4.4 The network based statistic

In order to compare the connectivity matrices of the different subject groups a t-statistic was computed for each unique connection (each element in one of the diagonal halves of the connectivity matrix) between the healthy control group and one of the MCI groups. The t-statistics were computed using a one-tailed t-test while assuming equal variances. Three different thresholds on the t-value were used ($t_{thresh} = 3.0$, $t_{thresh} = 3.5$ and $t_{thresh} = 4.0$) to exclude all links deemed to not have a strong enough contrast between the two populations. The thresholds were chosen through trial and error. The use of a positive threshold on the t-value determines the directionality of the change in contrast, excluding cases where the connectivity is strengthened in the MCI group compared to controls. Here, only connections that are weakened due to MCI are considered to be of interest. This creates a binary "map" of connections significantly weakened in the MCI group compared to the healthy controls. An example obtained with synchronization likelihood can be seen in Fig. 10.

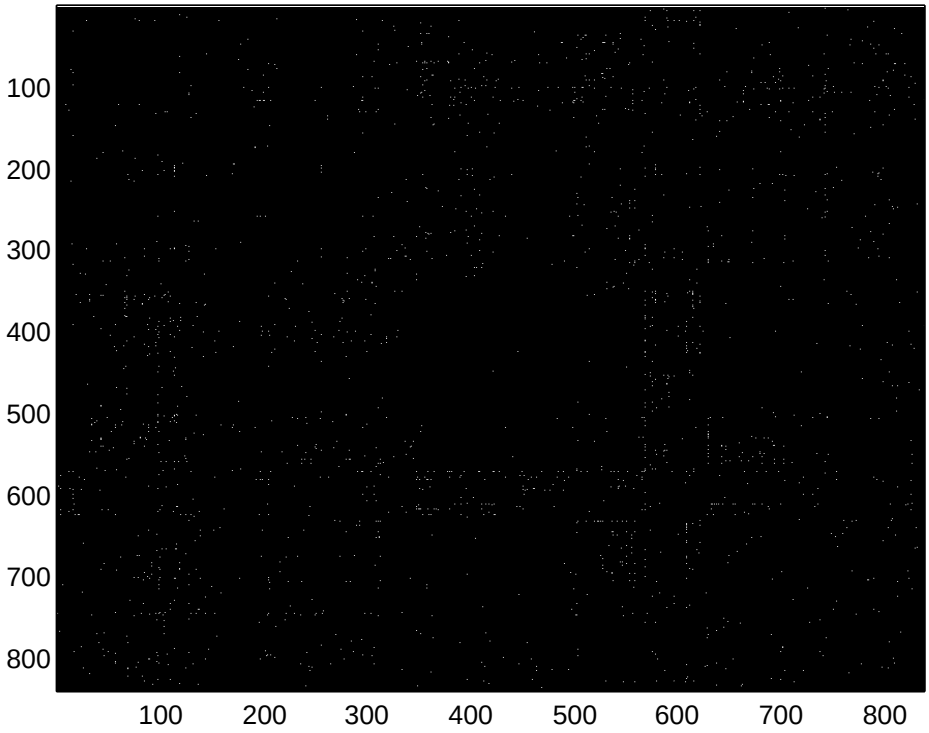

Figure 10: Connections between nodes with a contrast higher than $t_{thresh} = 3$ between healthy controls and 1A. Obtained with synchronization likelihood (m=9, w=9, vector distance calculated using the correlation distance, $FD_{mean} < 0.7mm$. Note the horizontal and vertical lines of weakened connections that intersect around node 600. This area is close to the caudate nucleus and thalamus, meaning these areas appear to have lost functionality in 1A compared to controls.

The extreme number of t-statistics ($\frac{840\times(840-1)}{2} = 352380$) calculated in this manner results in a map riddled with false positives i.e. the multiple comparison problem.

Because of this, a Network Based Statistic (NBS) method as described by Zalesky et al. was applied[15]. The individual contrast connections are grouped into "components". These components are simply obtained by assigning every node in the binary connectivity matrix (Fig. 10) connected to any other node through any number of intermediate nodes to one specific component.

For instance: node A is connected to node B but not to node C. Node B, however, is connected to node C. Therefore, a component consisting of node A, B and C is formed, see Fig. 11.

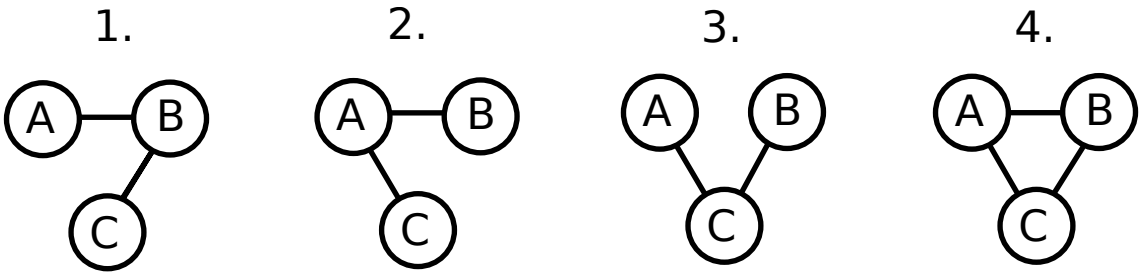

Figure 11: Four different alternatives of how a component consisting of three nodes can look. The size of the component is decided by the number of links it is comprised of. Component 4 has thus size three while components 1,2,3 has a size of two.

The size of each component obtained in this manner was then defined as the total number of links it comprised. The statistical significance of each component was then tested. This was done by pooling the two relevant subject groups and forming two new groups of the same sizes as the previous groups but each comprised of a random set of subjects. The size of the largest contrast component was then computed in the same manner as described above and added to a null distribution. This was done 10 000 times for each group comparison and/or mathematical approach. For the systems under consideration this generally results in p-values converging to two significant figures. 'Null' in null distribution refers to the null hypothesis being true, i.e. there is no difference in connectivity between the two groups, which of course is the case when each subject is assigned to one of the two groups randomly. A p-statistic was then obtained for each contrast component as the fraction of contrast components in the zero distribution larger than (or equal to) the contrast component being tested. This way, a statistical multiple comparison correction is not needed since we are just asking one question: "Is the size of the computed contrast component statistically significant?". The components were deemed significant for $p < 0.05$. Here, the p-value indicates the likelihood to obtain a component of that size provided there is no network contrast between the group in question and the controls. It is important to note that each individual link in the component can not be termed as being significantly different on its own, only the component as a whole[15]. An illustration of the approach derived from the binary connectivity matrix in Fig. 10 can be seen in Fig. 12.

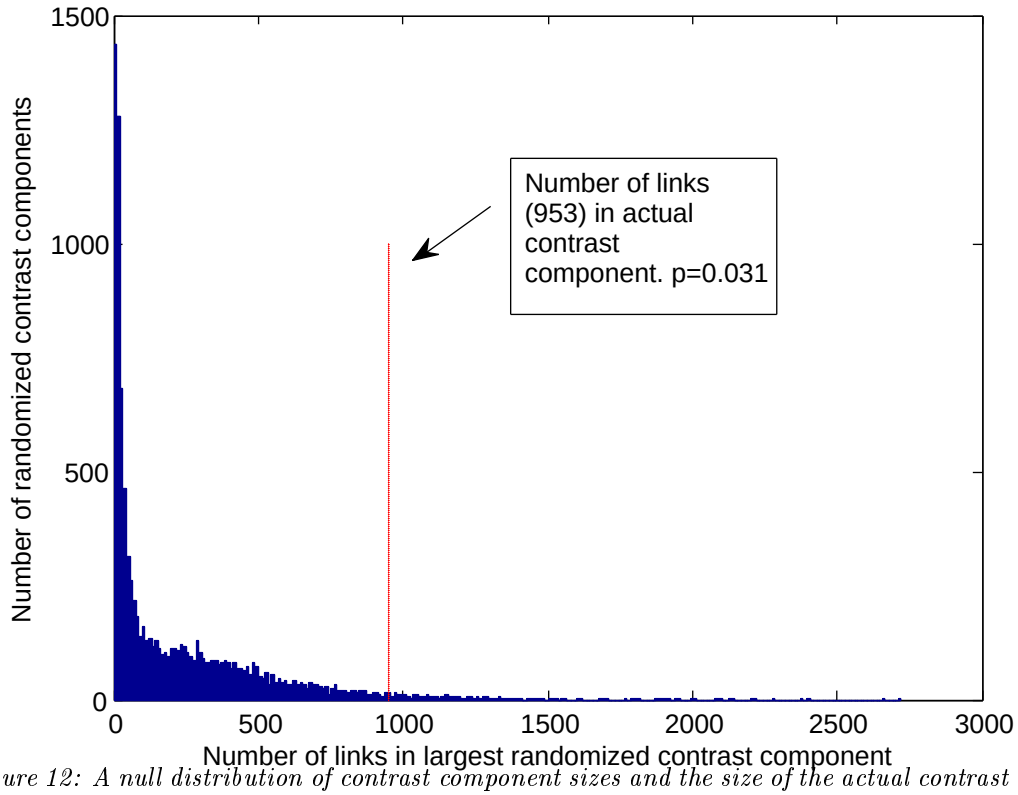

Figure 12: A null distribution of contrast component sizes and the size of the actual contrast component obtained when 1A and healthy controls were compared. The fraction of randomized component sizes greater than the size of the actual component (red line) determines the components p-value. The contrast component is deemed significant with p=0.031. Obtained with synchronization likelihood (m=9, w=9, vector distance calculated using the correlation distance, $FD_{mean} < 0.7mm$.

Note that the NBS approach does not correct for the FamilyWise Error Rate (FWER) in the strong sense, that is, the risk of committing at least one type 1 error (false positive) throughout all the hypotheses. The node-node links are, individually, not statistically significant. The p-values only speaks to whether the contrast component is significantly larger than the components obtained with randomized groups. The FWER is controlled in the weak sense however meaning that the FWER is controlled if all null hypotheses are true (all potential links are non-significant).

Because of the lack of readability in figures such as Fig. 10 each contrast component was also visualized using a 3D representation of the network. In these figures, the ROIs (displayed in Fig. 3) are represented by a node centered in each ROI. The size and color intensity of each node represents the number of links connected to it, the so called 'nodal degree'. The five nodes with the highest nodal degree received a label. These labels correspond to the x- and y axis in Fig. 10 defining the nodes anatomical position. The functional ROIs corresponding to each node are positioned, entirely or in part, inside one or two macro-anatomical units (for instance the hippocampus) defined in the AAL anatomical atlas[30]. If a node is marked with "*" it could not be found in the AAL and its anatomical overlap is instead defined by the Harvard-Oxford subcortical structural atlas. For each of the three connectivity measures, contrast components were visualized at the QA and t-statistic threshold deemed to provide the most satisfactory results for each measure.

4.4.5 Graph theoretical centrality measures

As a complement to calculating and visualizing entire networks, graph theoretical centrality measures can be applied unto the connectivity matrices.

In graph theory, different kinds of 'centrality' measures can be used to calculate the importance/relevance of each node in the graph[36]. When using graph theoretical centrality measures, no contrast components in between subject groups are obtained as is the case with the NBS approach. Thus, no networks are visualized using this method.

Centrality measures explore topological properties of the graph (connectivity matrix). The connectivity values remain undirected but now remain weighted (Fig. 4) instead of being thresholded and turned binary (Fig. 10. These centrality measures are also not defined for negative values since the connectivity values are seen as distances between the nodes in the graph[37]. Thus, when implementing them on connectivity matrices computed with correlation, negative connectivity values were set to zero.

One of these measures is the eigenvector centrality measure, previously implemented on rs-fMRI data by Lohman et al. [37]. A connectivity matrix, A, contains a set of n eigenvalues, λ_i, each corresponding to an eigenvector, $\vec{q_i} = \vec{q}_{i,1}, \vec{q}_{i,2}, ..., \vec{q}_{i,n}$, following the eigenvalue equation:

$$A\vec{q_i} = \lambda_i \vec{q_i}. \tag{20}$$

Because the graph is square and composed only of positive values there exists, according to the Perron-Frobenius theorem, a unique largest real eigenvalue with a corresponding eigenvector composed solely of positive elements[31,37]. Given that the eigenvalues of A are arranged in descending order of magnitude, $\lambda_1 \geq \lambda_2 \geq ... \geq \lambda_n$, the centrality of a node, v_i, is defined as the value of the corresponding element, $q_{1,i}$, in the dominant eigenvector, $\vec{q_1}$, that is, the eigenvector corresponding to the largest eigenvalue, λ_1.

In order for a node to achieve a high eigenvector centrality value it is not enough for it to have a lot of strong connections to other nodes. The other nodes it connects to *also* has to have strong connections to other nodes. The measure is self-referential, because high centrality is assigned to nodes referenced by other, highly central nodes. In other words, the centrality of each node is dependent on the centrality of each other node it is connected to. A variant of the eigenvector centrality is used in Google's PageRank" algorithm to list the most relevant hits for a search with very few iterations.

A simpler centrality measure is the 'strength' measurement. The strength, S, of a certain node, v_i, is the sum of all the weighted connectivity values, e, that node has to all other $n-1$ nodes:

$$S_i = \sum_{\substack{j=1 \\ j \neq i}}^{n-1} e_{i,j}. \tag{21}$$

Whether the change in centrality between a specific subject group and controls was significant was tested with the non-parametric Mann-Whitney U-test which does not assume normal distribution and has a wider applicability. Multiple comparison correction was performed using either the Bonferroni correction [38] on the 210 nodes with the largest mean centrality (across all subjects and subject groups) or the False Discovery Rate (FDR) controlling Benjamini-Hochberg procedure [38] on all nodes.

The Bonferroni correction is (in contrast to the NBS) designed to correct for the FWER thus making it a very conservative way to make a multiple comparison correction. Controlling the FWER means to control the risk of committing a type I (false positive) error at all throughout all hypotheses.

The correction is made simply by assigning significance at a level proportional to the number of hypotheses made. Thus, if significance normally would be assigned at $p<0.05$ it is now assigned at $p < \frac{0.05}{210}$.

Controlling the FDR is a less stringent multiple comparison correction than to control the FWER. When controlling the FDR the ratio of falsely rejected null hypotheses to correctly rejected hypotheses is controlled. A gain in power is thus obtained at the cost of specificity. The FWER is also controlled in the weak sense.

Controlling the FDR can be done by using the Benjamini-Hochberg procedure[38]. The p-values for each of the m hypotheses are arranged in increasing order, $p = p_1, p_2, ..., p_m$. Now let k be the highest index of p where:

$$p_k \leq \frac{k}{m}\alpha \tag{22}$$

is true and reject all null-hypotheses $(H_{0,1}, H_{0,2}, ..., H_{0,k})$ corresponding to p-values up to the k-index. α is the designated FDR that is, the allowed risk of falsely rejecting a null hypothesis.

Each p-value is in effect corrected in order to strengthen the discrimination against false positives based upon the number of tests versus the number of low p-values:

$$p_k \frac{m}{k} = p_{k,corrected} \leq \alpha. \tag{23}$$

This embodies the notion that a false positive among a small number of tests is more serious than for a large number of tests.

Results

5.1 The NBS approach

The statistical significance of the size of the contrast components computed in Sec. 4.4.4 can be seen in tables 2 and 3. p-values for each QA, threshold on the t-statistic, group comparison and connectivity measure is presented. From the tables it is evident that the subjective MCI group with Aβ42$\leq$647 ng/l (1A) has the clearest most distinguishable reduction in connectivity while the contrast in the objective MCI group with P-τ>70 ng/l (2B) is completely absent. The subjective MCI group with high P-τ (1B) and the objective MCI group with low Aβ42 (2A) generally fall in between the other two MCI groups (1A and 2B) when it comes to statistical significance. These results are somewhat contradictory to the progression hypothesis described in Sec. 4.1 where objective MCI and high P-τ is connected to an increased pathology i.e. an overall decrease of cognitive function.

Correlation obtains larger contrast components and has a generally stronger statistical power than synchronization likelihood and mean phase coherence. Results from the two QA:s are generally very similar and any differences between them could be ascribed to chance. Raising the threshold on the t-statistic is a double-edged sword when it comes to the statistical power since it decreases the number of statistically significant links in both the actual contrast component and the randomized contrast components it is compared to, Fig. 12. Lowering the the threshold on the t-statistic is also a double-edged sword since the size of randomized components will increase as well as the size of the actual contrast components. A threshold on the t-statistic of 3.0 or 3.5 appears to give similar results while a threshold on 4.0 discriminates so much that the results are severely weakened.

Networks of weakened connectivity based on the contrast components in tables 2 and 3 are visualized in Figs. 13, 14 and 15. For each connectivity measure, the QA and the threshold on the t-statistic, deemed to provide the most satisfactory results were used for the visualization of the weakened network. Each functionally distinct ROI described in Sec. 4.3 is represented by a node and placed in an MNI brain template as described in Sec. 4.4.4. The five nodes in each network with the highest nodal degree are labeled. Each label corresponds to one or two macro-anatomical units defined by the AAL atlas. If a node is marked with a "*" its macro-anatomical affinity is instead defined by the Hardvard-Oxford Subcortical Structural Atlas.

Only correlation was able to find significant networks in three group comparisons for the same QA and threshold. The networks comparing 1A with controls are overall quite similar with the weakening centered around primarily the thalamus and caudate nucleus regions. Synchronization likelihood however, detects a weakened connection to the frontal middle gyrus while correlation and mean phase coherence has a bigger focus towards the posterior regions, mainly the cerebellum. When comparing 1B to controls, mean phase coherence and correlation again display resembling results. Just as when comparing 1A to controls the weakened network is centered around the thalamus and caudate nucleus with some connections to the more posterior regions. The weakened connectivity of the thalamus in MCI subjects has previously been established by, for instance, Wang et al. using rs-fMRI[39].

In the objective MCI group, 2A, the network configuration changes and shifts focus from the thalamus and caudate nucleus to the posterior cingulate but mainly the hippocampal regions. This relationship is more true when using correlation. When using synchronization likelihood, the shift in focus is not as clear. There exists more of an overlap with the weakened network that appears in the subjective MCI groups. The weakening of the thalamus is still quite dominant but a gradual shift of the weakening connectivity seems to have moved in a caudal direction towards the hippocampus. The weakened connectivity between the hippocampus and the posterior cingulate

gyrus in MCI and early AD has previously been found by Zhou et al. using fMRI and diffusion tensor imaging[40].

Finally, the most prominent of the 840 ROIs for each group comparison across all connectivity measures are visualized in cross sections of the MNI brain in Figs. 16, 17 and 18 to present their anatomical position in an alternate, hopefully clearer, way.

Table 2: Significance of contrast components between controls and each MCI group with $FD_{mean} < 0.5mm$. The contrast components of the three connectivity measures for different thresholds of the t-statistic. Significant contrast components ($p < 0.05$) are marked green. Contrast components on a 'trend-level' ($0.05 \leq p < 0.1$) are marked pink. Insignificant contrast components ($p \geq 0.1$) are marked red. The amount of links a contrast component was composed of is presented if it was deemed significant or to show a trend level.

Threshold on t	Groups	Measure	p-value	Links
3.0	1A-Controls	Synchronization likelihood	0.0067	1013
		Mean phase coherence	0.0056	2483
		Correlation	0.0019	5880
	1B-Controls	Synchronization likelihood	0.15	-
		Mean phase coherence	0.12	-
		Correlation	0.014	3620
	2A-Controls	Synchronization likelihood	0.055	757
		Mean phase coherence	0.15	-
		Correlation	0.057	1864
	2B-Controls	Synchronization likelihood	0.65	-
		Mean phase coherence	0.70	-
		Correlation	0.77	-
3.5	1A-Controls	Synchronization likelihood	0.016	16
		Mean phase coherence	0.0043	557
		Correlation	0.0013	1789
	1B-Controls	Synchronization likelihood	0.74	-
		Mean phase coherence	0.044	81
		Correlation	0.0090	1083
	2A-Controls	Synchronization likelihood	0.063	13
		Mean phase coherence	0.20	-
		Correlation	0.043	463
	2B-Controls	Synchronization likelihood	0.79	-
		Mean phase coherence	0.60	-
		Correlation	0.84	-
4.0	1A-Controls	Synchronization likelihood	0.12	-
		Mean phase coherence	0.0039	40
		Correlation	<0.001	429
	1B-Controls	Synchronization likelihood	0.79	-
		Mean phase coherence	0.066	-
		Correlation	0.0035	310
	2A-Controls	Synchronization likelihood	0.96	-
		Mean phase coherence	0.16	-
		Correlation	0.026	80
	2B-Controls	Synchronization likelihood	1.0	-
		Mean phase coherence	0.87	-
		Correlation	0.90	-

Table 3: Significance of contrast components between controls and each MCI group with $FD_{mean} < 0.7mm$. The contrast components of the three connectivity measures for different thresholds of the t-statistic. Significant contrast components ($p < 0.05$) are marked green. Contrast components on a 'trend-level' ($0.05 \leq p < 0.1$) are marked pink. Insignificant contrast components ($p \geq 0.1$) are marked red. The amount of links a contrast component was composed of is presented if it was deemed significant or to show a trend level.

Threshold on t	Groups	Measure	p-value	Links
3.0	1A-Controls	Synchronization likelihood	0.031	953
		Mean phase coherence	0.031	1744
		Correlation	0.0065	4820
	1B-Controls	Synchronization likelihood	0.67	-
		Mean phase coherence	0.52	-
		Correlation	0.085	1534
	2A-Controls	Synchronization likelihood	0.043	838
		Mean phase coherence	0.13	-
		Correlation	0.062	1733
	2B-Controls	Synchronization likelihood	0.53	-
		Mean phase coherence	0.62	-
		Correlation	0.70	-
3.5	1A-Controls	Synchronization likelihood	0.012	59
		Mean phase coherence	0.016	414
		Correlation	0.0031	1522
	1B-Controls	Synchronization likelihood	0.80	-
		Mean phase coherence	0.61	-
		Correlation	0.053	401
	2A-Controls	Synchronization likelihood	0.055	16
		Mean phase coherence	0.21	-
		Correlation	0.044	433
	2B-Controls	Synchronization likelihood	0.78	-
		Mean phase coherence	0.73	-
		Correlation	0.87	-
4.0	1A-Controls	Synchronization likelihood	0.035	3
		Mean phase coherence	0.0061	49
		Correlation	0.0021	370
	1B-Controls	Synchronization likelihood	0.82	-
		Mean phase coherence	0.85	-
		Correlation	0.024	90
	2A-Controls	Synchronization likelihood	0.93	-
		Mean phase coherence	0.097	5
		Correlation	0.039	46
	2B-Controls	Synchronization likelihood	0.80	-
		Mean phase coherence	0.84	-
		Correlation	0.88	-

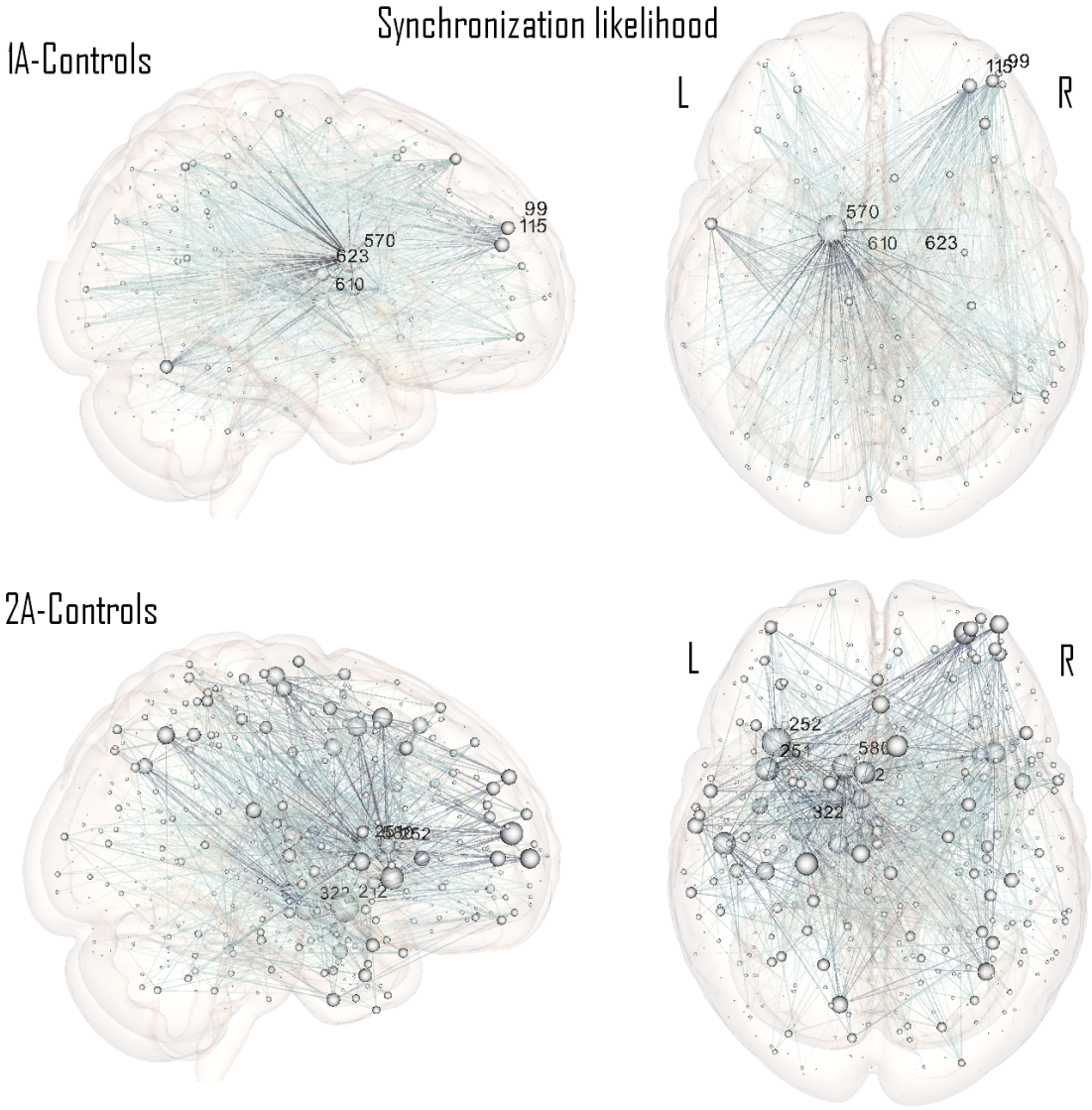

Figure 13: Contrast components obtained using synchronization likelihood between controls and, from top to bottom: 1A (subjective MCI, Aβ42≤647 ng/l) and 2A (objective MCI, Aβ42≤647 ng/l). Threshold on the t-statistic of 3.0 and $FD_{mean} < 0.7mm$. Marked nodes are in ***1A-Controls:*** *99(100 % middle frontal gyrus, R), 115(82 % middle frontal gyrus, R), 570(82 % caudate nucleus, L), 610(91 % thalamus, L) and 623(92% thalamus, R). Marked nodes are in* ***2A-Controls:*** *212*(37 % cerebral cortex, L), 251(72 % insula, L), 252(77 % insula, L), 322(67 % hippocampus, L) and 580(79 % caudate nucleus, L). *=Harvard-Oxford subcortical structural atlas*

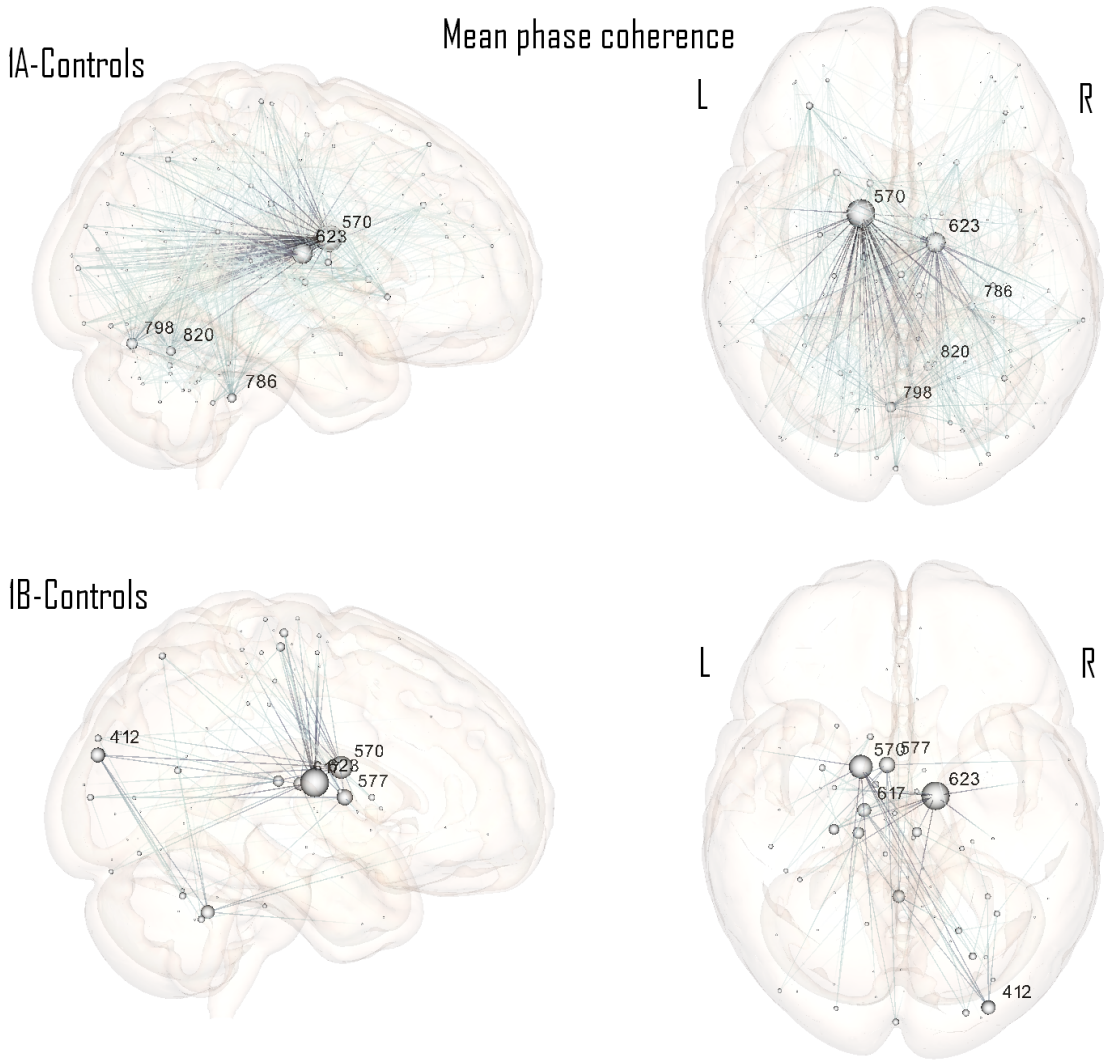

Figure 14: Contrast components obtained using mean phase coherence between controls and, from top to bottom: 1A (subjective MCI, Aβ42$\leq$647 ng/l) and 1B (subjective MCI, P-τ>70 ng/l). Threshold on the t-statistic of 3.5 and $FD_{mean} < 0.5mm$. Marked nodes are in ***1A-Controls:*** *570(82 % caudate nucleus, L), 623(92% thalamus, R), 786(23% hemisperic lobule X, cerebellum, R), 798(45% hemispheric lobule VI, cerebellum, L and 20% crus I, cerebellum, L) and 820(30 % hemispheric lobule VI, cerebellum, R) Marked nodes are in* ***1B-Controls:*** *412(65 % middle occipital gyrus, R, and 35 % superior occipital gyrus, R), 570(82 % caudate nucleus, L), 577*(72 % thalamus, L), 617(95 % thalamus, L) and 623(92% thalamus, R). *=Harvard-Oxford subcortical structural atlas*

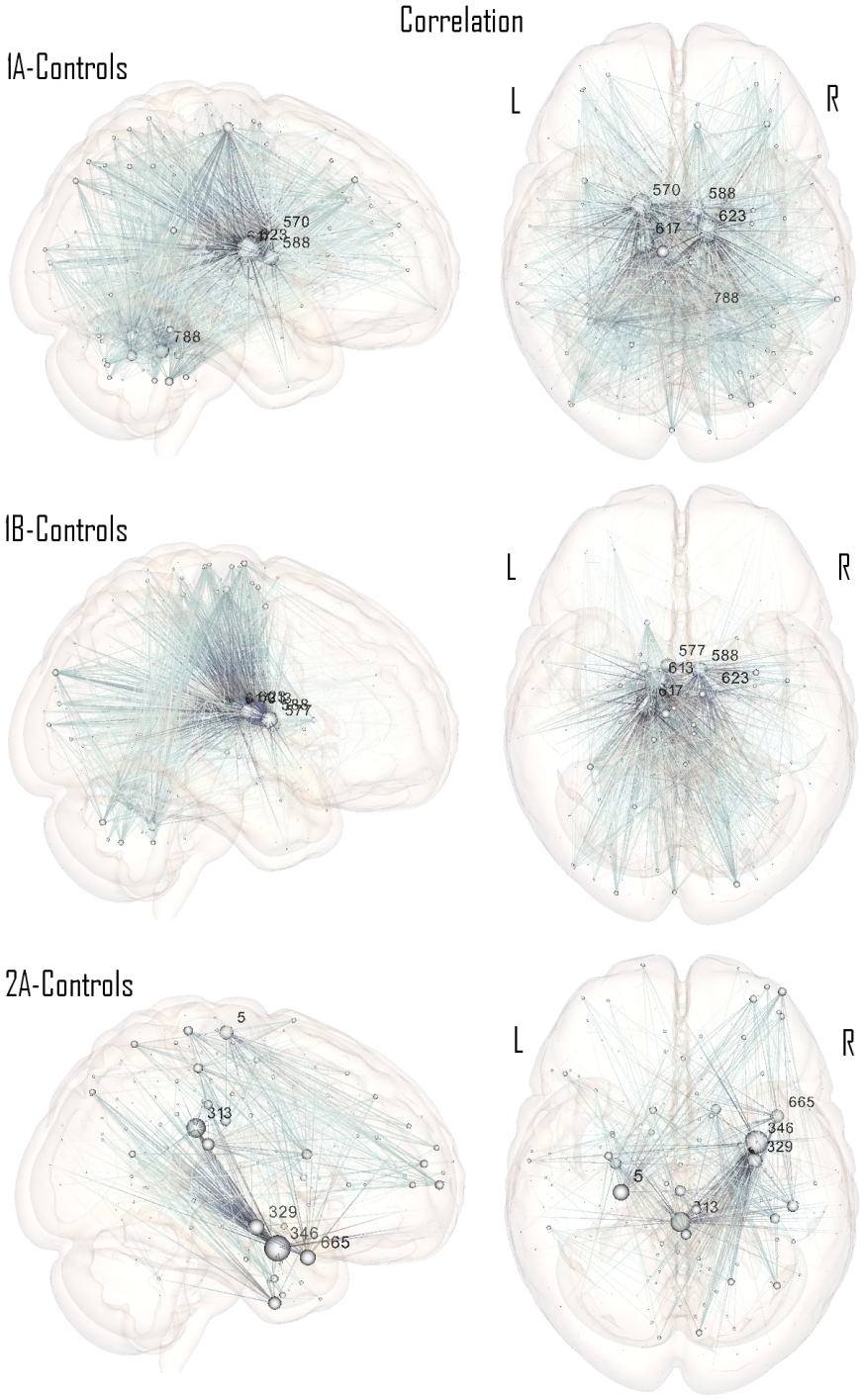

Figure 15: Contrast components obtained using correlation between controls and, from top to bottom: 1A (subjective MCI, Aβ42$\leq$647 ng/l), 1B (subjective MCI, P-τ>70 ng/l) and 2A (objective MCI, Aβ42$\leq$647 ng/l). Threshold on the t-statistic of 3.5 and $FD_{mean} < 0.5$mm. Marked nodes are in ***1A-Controls:*** *570(82 % caudate nucleus, L), 588*(98 % thalamus, R), 617(95 % thalamus, L), 623(92% thalamus, R) and 788*(3 % brain stem). Marked nodes are in* ***1B-Controls:*** *577*(72 % thalamus, L), 588*(98 % thalamus, R), 613(63 % thalamus, L), 617(95 % thalamus, L) and 623(92% thalamus, R). Marked nodes are in* ***2A-Controls:*** *5(69 % precentral gyrus, L), 313(35 % posterior cingulate gyrus, L), 329(51 % hippocampus, R), 346(40 % amygdala, R, and 35 % hippocampus, R) and 665(65 % temporal pole, superior temporal gyrus, R). *=Harvard-Oxford subcortical structural atlas*

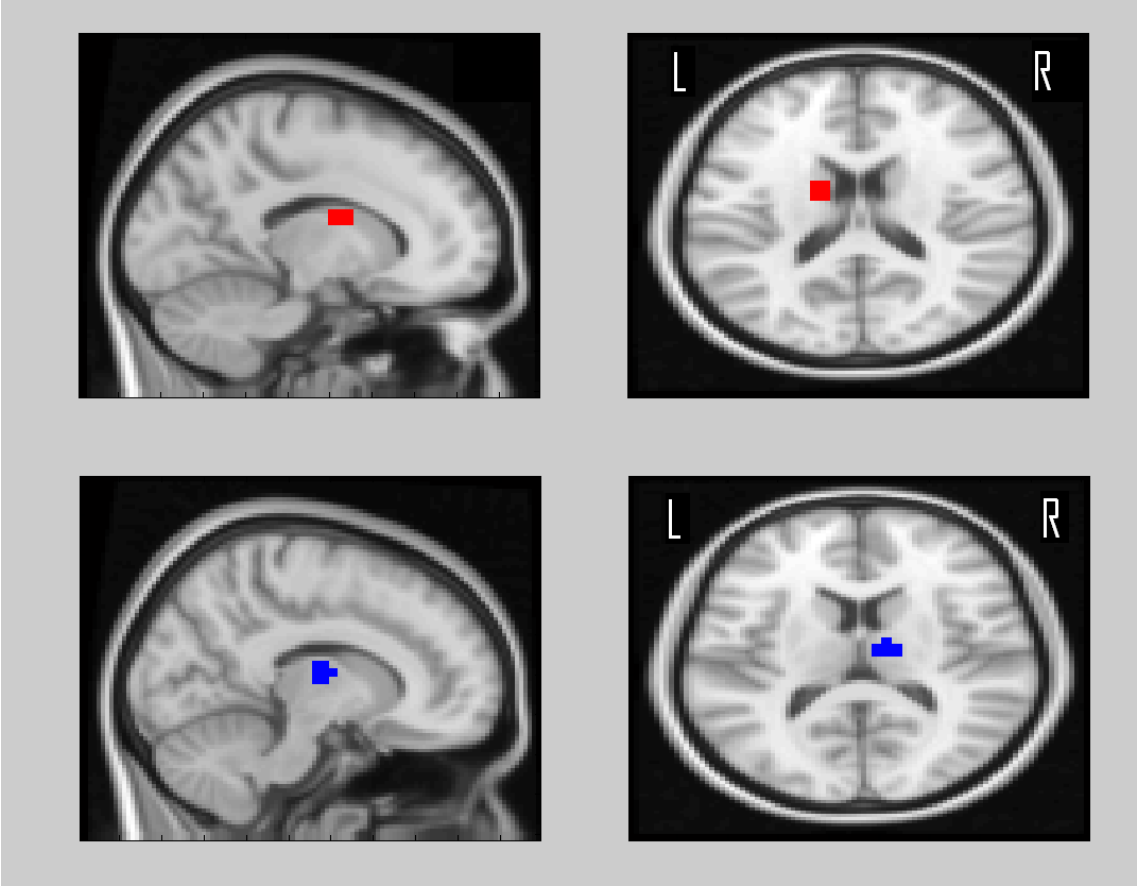

Figure 16: The ROI colored in red (#570) overlaps with the caudate nucleus, L, to 85%. The ROI colored in blue(#623) overlaps with the thalamus, R, to 92%. Both ROIs appeared to be weakened in the subjective MCI group 1A.

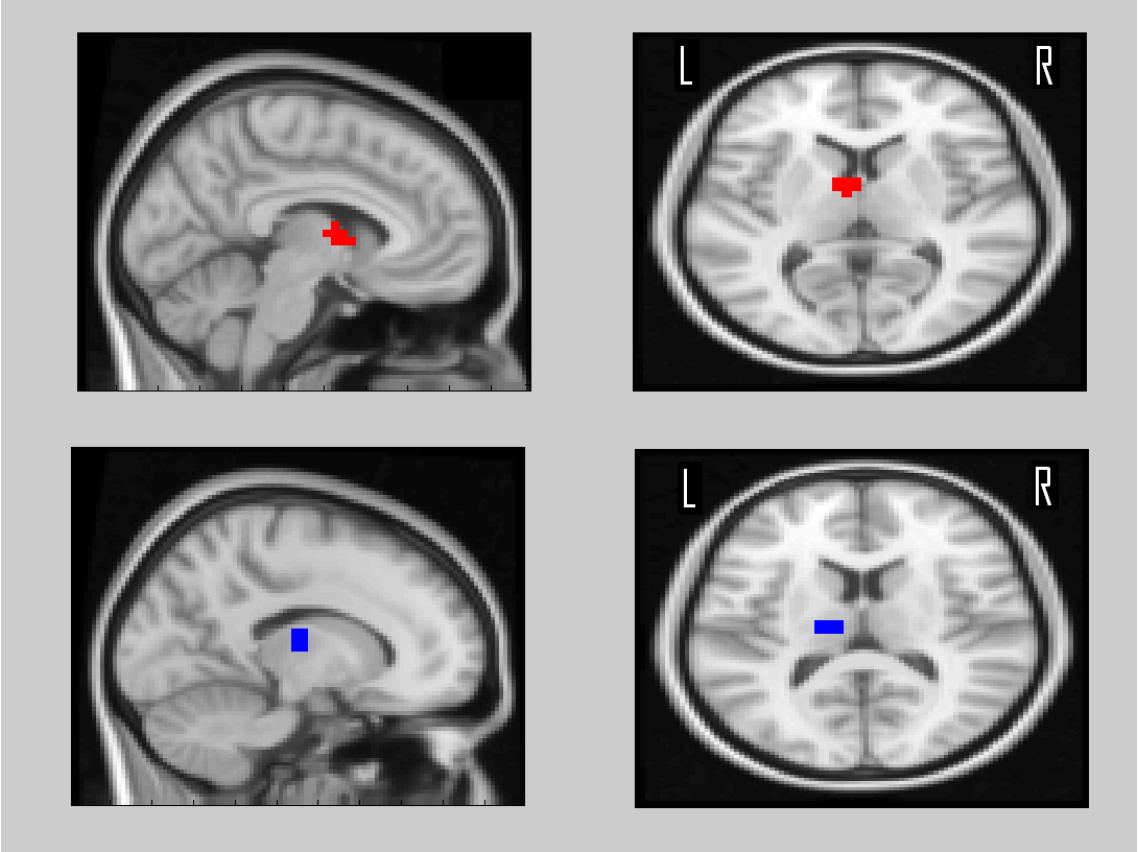

Figure 17: The ROI colored in red (#577) overlaps with the thalamus, L, to 72%. The ROI colored in blue (#617) overlaps with the thalamus, L, to 95%. Both ROIs appeared to be weakened in the subjective MCI group 1B. *=Harvard-Oxford subcortical structural atlas*

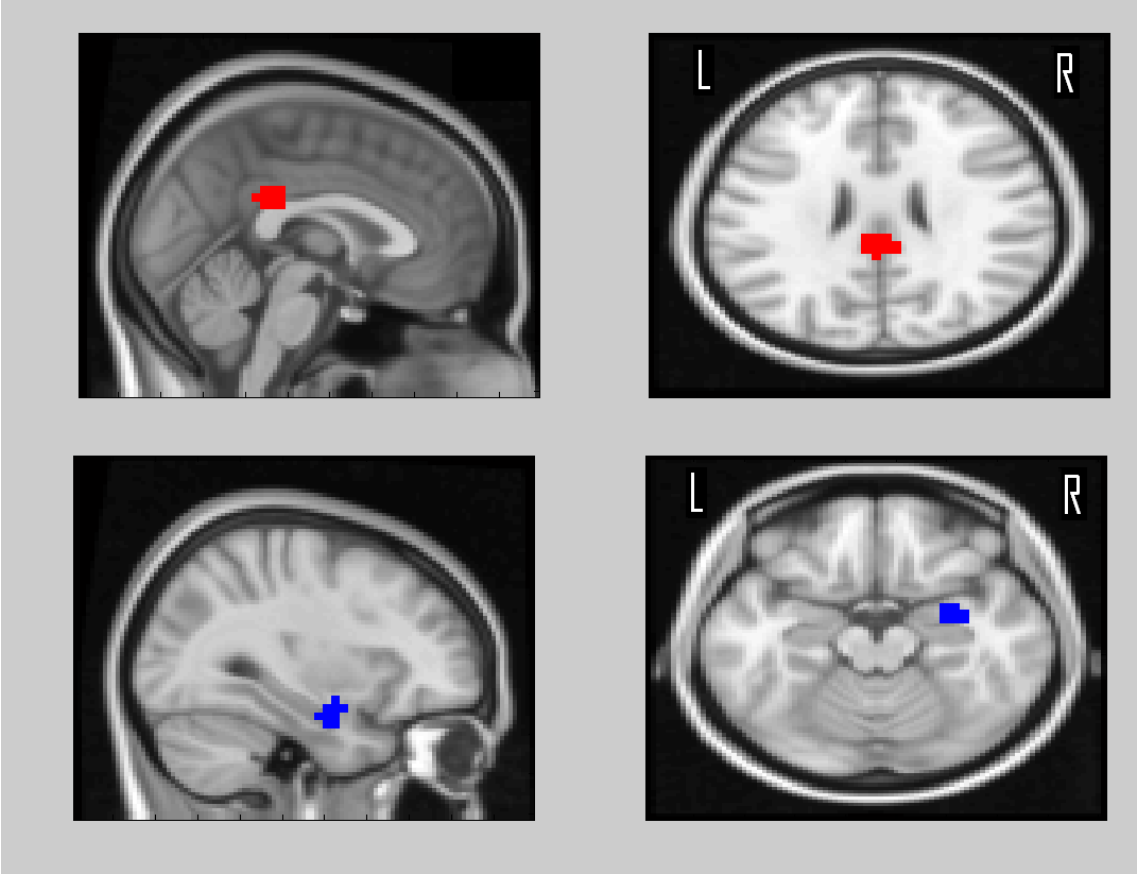

Figure 18: The ROI colored in red (#313) overlaps with the posterior cingulate gyrus, L, to 35%. The ROI colored in blue (#346) overlaps with the amygdala, R, to 40% as well as the hippocampus, R, to 35%. Both ROIs appeared to be weakened in the objective MCI group 2A.

5.2 Centrality measures

Nodes with significantly changed centrality (strength or eigenvector centrality) are shown in tables 4 and 5, see Sec.4.4.5. Nodes with a weakened connectivity compared to controls are marked with a "w" while nodes with a strengthened connectivity compared to controls are marked with an "s". In table 4 the FDR is controlled using the Benjamini-Hochberg procedure while in table 5 the FWER is controlled using the Bonferroni method for the 210 nodes with the largest change in centrality. Regardless of the statistical test used, only nodes in the subjective MCI group 1A have a significant change in centrality compared to healthy controls. As can be seen, controlling for the FDR achieves higher statistical power even though only a quarter of the total amount of nodes are taken into account when controlling for the FWER.

The connectivity measures obtains somewhat similar results although correlation detects some weakened nodes in the cerebellum using strength and $FD_{mean} < 0.5$ mm in table 4 concordant with results using the network based statistic. Synchronization likelihood and mean phase coherence detects an interesting effect when using eigenvector centrality and $FD_{mean} < 0.7$ mm, also in table 4. The olfactory cortex, associated with the sense of smell and smell related memories, have obtained a compensatory effect meaning it has a stronger connectivity in the MCI subgroup compared to healthy controls.

No significance is obtained when using eigenvector centrality and $FD_{mean} < 0.5$ mm. This is possibly due to that the self-referential nature of the centrality measure demands a higher amount of links than strength to depict the topological structure of the network. With a harsher QA, the group sizes decrease and thus the noise level increase resulting in overall lower t-values in the subject group comparison.

The weakening of the thalamus and caudate nucleus in the subjective MCI group 1A is well in

concordance with the results using the network based statistic.

In table 5, using correlation, strength and $FD_{mean} < 0.7$ mm both a weakening and a strengthening is detected in the thalamus for two different nodes. This could possibly be due to poor specificity of the correlation measure, causing it to detect artifacts. Eigenvector centrality is not defined for negative connectivities and all negative values are thus not considered which could play a part in this observation.

*Table 4: Nodes with a significant ($p<0.05$) change in strength or eigenvector centrality in MCI group 1A ($A\beta 42 \leq 647$ ng/l, subjective MCI) compared to controls. A strengthening in centrality of the node is denoted by "s" while a weakening is denoted by "w". Multiple comparison correction performed with Benjamini-Hochberg FDR. *=Harvard-Oxford subcortical structural atlas*

	Strength	
	$FD_{mean} < 0.7$ mm	$FD_{mean} < 0.5$ mm
Synchronization likelihood	Caudate nucleus (570-w) Thalamus (610-w)	Caudate nucleus (570-w)
Mean phase coherence	Caudate nucleus (570-w) Thalamus (610-w)	Caudate nucleus (570-w) Thalamus (623-w)
Correlation	Caudate nucleus (570-w) Thalamus (577*-w, 588*-w, 610-w, 613-w, 623-w)	Caudate nucleus(570-w) Thalamus (588*-w, 610-w, 613-w, 617-w, 623-w) Cerebellum(755-w, 799-w, 801-w, 802-w, 806-w) Brain Stem(788*-w)
	Eigenvector centrality	
	$FD_{mean} < 0.7$ mm	$FD_{mean} < 0.5$ mm
Synchronization likelihood	Olfactory cortex (211-s) Caudate nucleus (570-w, 580-w) Thalamus (577-w, 610-w)	-
Mean phase coherence	Olfactory cortex (211-s) Caudate nucleus (570-w, 580-w) Thalamus (610-w, 617-w, 620-w, 623-w)	-
Correlation	Caudate nucleus (570-w) Thalamus (623-w)	-

*Table 5: Nodes with a significant ($p<0.05$) change in strength and eigenvector centrality in MCI group 1A ($A\beta 42 \leq 647$ ng/l, subjective MCI) compared to controls. A strengthening in centrality of the node is denoted by "s" while a weakening is denoted by "w". Multiple comparison correction performed with the Bonferroni method. Only the 210 nodes (25%) with the highest centrality value tested. *=Harvard-Oxford subcortical structural atlas*

Strength		
	$FD_{mean} < 0.7$ mm	$FD_{mean} < 0.5$ mm
Synchronization likelihood	-	-
Mean phase coherence	-	Thalamus (623-w)
Correlation	Thalamus (610-w, 623-s)	Thalamus (588*-w, 623-w)
Eigenvector centrality		
	$FD_{mean} < 0.7$ **mm**	$FD_{mean} < 0.5$ **mm**
Synchronization likelihood	-	-
Mean phase coherence	Thalamus (623-w)	-
Correlation	Thalamus (623-w)	-

Discussion

6.1 The NBS approach

Between MCI subject groups, the one that consistently deviates in functionality from the controls for almost all tests is 1A. i.e. subjects with subjective MCI and low Aβ42. The clearer difference in functionality for this group compared to the groups with high P-τ (1B and 2B) could simply be a result from the larger sample size of 1A, see table 1. Also, the inclusion of subjects with Aβ42 levels above 647 ng/l in 1B and 2B could possibly be inappropriate, only serving to weaken the contrast to controls. The apparent clearer contrast in the subjective groups (1A and 1B) compared to the objective groups (2A and 2B) is not as easily explained however. Intuitively, the objective MCI subject groups could be expected to show a higher contrast due to their more advanced pathology. A possible reason for this observation could be a higher 'within group variance' in the structure of the functional networks for the subjects in the objective MCI groups, making the contrast to controls more diffuse. Possibly, the variation in tissue atrophy is so large in the objective MCI groups that the normalization to the MNI brain becomes "smeared" causing noise. Note that no contrast whatsoever was found in 2B (objective MCI, high P-τ), which could be considered consisting of subjects with the most severe form of cognitive impairment in this project. This may be because of a combination of the two above stated reasons.

A recurring theme throughout the project was a weakening in connectivity to/from, above all, the thalamus, but also in the caudate nucleus in accordance with Wang et al.[39] for the subjective MCI groups while 2A showed a weakening to/from mainly the hippocampus but also the amygdala and the posterior cingulate gyrus in accordance with Zhou et al[40]. The latter contrast only appears when using correlation while the former consistently appears using all methods.

It is evident that correlation has a higher sensitivity than the other connectivity measures. It consistently obtains lower p-values and finds more significant links in each component than the other connectivity measures. This could be both something positive as well as something negative. It is hard to say whether correlation obtains the lowest p-values due to a high sensitivity or a low specificity. Correlation however, obtain consistent results regarding diminishing functionality in the hippocampus of subjects with objective MCI (2A) which is in accordance with previous studies related to MCI[40–42].

Synchronization likelihood has a stronger statistical power when the less strict QA of $FD_{mean} <$ 0.7 mm is used contrary to correlation and mean phase coherence. This is perhaps due to the more

complex nature of synchronization likelihood meaning it needs a larger subject group in order to discern a pattern. Synchronization likelihood is very dependent on being able to construct a large number of time embedded vectors that can be compared to each other. When the time series, as in this case, are relatively short, group sizes most likely need to be increased to increase the statistical power.

In tables 2 and 3 a lot of p-values are presented, often in close proximity to the cut-off value of 0.05. It is therefor very important to note the arbitrary nature of this cut-off value. There exists no meaningful distinction between a p-value of 0.04 and one of 0.06 but the cut-off for significance has to be placed somewhere. All p-values have therefor been included instead of stating significance at a certain confidence interval so that readers may form their own opinion of the significance of the results.

With synchronization likelihood, three contrast components comparing controls and subjects with objective MCI (2A) fall into the trend-level interval. These contrast components, along with the one displayed in Fig. 13, appear to show a form of 'progression' of the MCI. The objective-controls networks show a larger degree of overlap with the subjective-controls network specifically displaying a lowered functionality in the thalamus. The reduced functionality in the thalamus for subjective MCI subjects becomes relatively less apparent for the objective MCI subjects when using correlation. This does not appear to be the case when using synchronization likelihood. It could be considered strange that regions of the brain, that previously had a lowered degree of functionality, regains (to some degree) that functionality as the MCI progresses. This could be an effect of the linear nature of the correlation operation. Of course, the view that the objective MCI groups represents a progression of the disease relative the subjective MCI groups is just a hypotheses. The difference between subjective and objective subjects displayed with correlation could very well be the proper relationship. It is possible that subjective and objective subjects displays different pathways of the disease meaning the senile plaques (Aβ42) first attacks the thalamus and caudate nucleus in the subjective subjects while targeting the hippocampal areas first in the objective subjects. It is reasonable to believe however, that it is the targeting of the hippocampus that affects the subjects in such a way that they perform poorly in the ADAS-3 congitive test.

Because the exact structure of the examined cognitive networks are not known it is difficult to determine what constitutes a good result. In future works, it could be of value to implement these connectivity measures on predetermined simulated networks as in Smith et al.[43].

In hindsight it could have been preferable to not assume equal variance between controls and MCI subject groups when calculating a t-statistic showing the change of connectivity between two nodes since there are no real indications such an assumption can be made. Alternatively, it may have been preferable to use the Mann-Whitney U-statistic since it does not assume normal distribution of the node-node connectivity across the subject group. The impact of these changes on the results are expected to just cause a light lessening of the statistical power.

Implementing a negative threshold on the t-statistic in order to search for strengthened, compensatory, networks would have been interesting. Strengthened nodes are however examined when using the graph theoretical centrality measures.

6.2 Graph centrality measures

All contrasts except 1A compared to controls were completely invisible using graph centrality measures. The nodes found to be weakened in 1A when using the centrality measures correlated well with those that were found using the NBS. The nodes are predominantly the thalamus and to a somewhat lesser degree, the caudate nucleus. Not surprisingly, strength and correlation discovers the highest amount of significantly changed nodes. Strength is a more direct measure than eigenvalue centrality and demands less when determining how much the centrality in a node has changed. Correlation, as was seen using the NBS approach, simply has a higher sensitivity than the other connectivity measures. Furthermore, the results depend heavily on the QA used. Not a single node was found to have a significant change with $FD_{mean}<0.5$ mm when eigenvector centrality was used. This could be due to eigenvector centrality being very dependent on a large material to be able to discern the centrality of the nodes.

The compensatory effect in the olfactory cortex detected using eigenvector centrality on the

synchronization likelihood and mean phase coherence matrices is quite interesting however.

Apart from this, the graph centrality measures did not add much information about the change in brain network connectivity that had not already been gained from the NBS approach.

Conclusion

Synchronization likelihood appears to have some valuable information to offer regarding the hypothesised progression of MCI that seems to be absent when using correlation. Intuitively, regions that are cognitively weakened in the subjective MCI groups should remain so in the objective MCI groups (thalamus, caudate nucleus) while new regions (for instance the hippocampus) also become weakened. A relationship that is somewhat satisfactory shown when using synchronization likelihood. Synchronization likelihood identifies the hippocampus as having a decreased cognitive function in 2A, same as with correlation but the areas around the caudate nucleus and thalamus are still quite central in the weakened network contrary to correlation. The overlap between subjective and objective MCI groups using synchronization likelihood could be a sing of progression.

The main issue with synchronization likelihood is the power. This is likely due to the limited amount of discrete time points used in each time series. 175 discrete time points were used in each time series which can be compared to studies involving EEG or MEG where samples number around 4000[10, 11, 44]. The limited amount of data points obtained with $TR = 2000$ ms could impair the measures ability to discover recurring patterns in between the time series. The most obvious way to improve the statistical power would be to decrease the TR in order to increase temporal resolution. An increased acquisition time would likely also increase the statistical power. Another way to possibly increase the power is multiband radiofrequency excitation where several slices are acquired using the same TR thus, in practice, improving the time resolution. Such studies have been performed using 7 T equipment by Moeller et al.[20]. It is the author's opinion that synchronization likelihood has the potential to become useful in future fMRI studies.

Mean phase coherence obtained similar results as correlation in the subjective groups. In the objective groups however mean phase coherence obtained no significant change in connectivity. This could possibly be a sign that the contrast in the objective MCI groups are, at least in part, due to some phase shift between the time series of the nodes.

References

[1] Ron Brookmeyer, Sarah Gray, and Claudia Kawas. Projections of Alzheimer's Disease in the United States and the Public Health Impact of Delaying Disease Onset. 1999.

[2] PK Mölsä, RJ Marttila, and UK Rinne. Survival and cause of death in Alzheimer's disease and multiâĂŘinfarct dementia. *Acta Neurologica ...*, (6):103–107, 1986.

[3] Ron Brookmeyer, Elizabeth Johnson, Kathryn Ziegler-Graham, and H Michael Arrighi. Forecasting the global burden of Alzheimer's disease. *Alzheimer's & dementia : the journal of the Alzheimer's Association*, 3(3):186–91, July 2007.

[4] John Markoff. Obama Seeking to Boost Study of Human Brain, 2013.

[5] M H Lee, C D Smyser, and J S Shimony. Resting-state fMRI: a review of methods and clinical applications. *AJNR. American journal of neuroradiology*, 34(10):1866–72, October 2013.

[6] M De Luca, C F Beckmann, N De Stefano, P M Matthews, and S M Smith. fMRI resting state networks define distinct modes of long-distance interactions in the human brain. *NeuroImage*, 29(4):1359–67, February 2006.

[7] Walter Koch, Stephan Teipel, Sophia Mueller, Jens Benninghoff, Maxmilian Wagner, Arun L W Bokde, Harald Hampel, Ute Coates, Maximilian Reiser, and Thomas Meindl. Diagnostic power of default mode network resting state fMRI in the detection of Alzheimer's disease. *Neurobiology of aging*, 33(3):466–78, March 2012.

[8] Zhengjia Dai, Chaogan Yan, Zhiqun Wang, Jinhui Wang, Mingrui Xia, Kuncheng Li, and Yong He. Discriminative analysis of early Alzheimer's disease using multi-modal imaging and multi-level characterization with multi-classifier (M3). *NeuroImage*, 59(3):2187–95, February 2012.

[9] Juan Zhou, Michael D Greicius, Efstathios D Gennatas, Matthew E Growdon, Jung Y Jang, Gil D Rabinovici, Joel H Kramer, Michael Weiner, Bruce L Miller, and William W Seeley. Divergent network connectivity changes in behavioural variant frontotemporal dementia and Alzheimer's disease. *Brain : a journal of neurology*, 133(Pt 5):1352–67, May 2010.

[10] C.J. Stam and B.W. van Dijk. Synchronization likelihood: an unbiased measure of generalized synchronization in multivariate data sets. *Physica D: Nonlinear Phenomena*, 163(3-4):236–251, March 2002.

[11] T Montez, K Linkenkaer-Hansen, B W van Dijk, and C J Stam. Synchronization likelihood with explicit time-frequency priors. *NeuroImage*, 33(4):1117–25, December 2006.

[12] J.A. Scott Kelso. Self-Organization of the Human Brain. In *Dynamic Patterns - The self-organization of brain and behavior*, pages 257–285. 1999.

[13] Florian Mormann, Klaus Lehnertz, Peter David, and Christian E. Elger. Mean phase coherence as a measure for phase synchronization and its application to the EEG of epilepsy patients. *Physica D: Nonlinear Phenomena*, 144(3-4):358–369, October 2000.

[14] Oskar Hansson, Henrik Zetterberg, Peder Buchhave, Elisabet Londos, Kaj Blennow, and Lennart Minthon. Association between CSF biomarkers and incipient Alzheimer's disease in patients with mild cognitive impairment: a follow-up study. *Lancet neurology*, 5(3):228–34, March 2006.

[15] Andrew Zalesky, Alex Fornito, and Edward T Bullmore. Network-based statistic: identifying differences in brain networks. *NeuroImage*, 53(4):1197–207, December 2010.

[16] Russel A. Poldrack, Jeanette A. Mumford, and Thomas E. Nichols. Statistical modeling: Single subject analysis. In *Handbook of functional MRI Data Analysis*, pages 70–99. Cambridge University Press, 2011.

[17] Russel A. Poldrack, Jeanette A. Mumford, and Thomas E. Nichols. *Handbook of FUNCTIONAL MRI Data Analysis*. Cambridge University Press, 2011.

[18] Randy L Buckner, Jessica R Andrews-Hanna, and Daniel L Schacter. The brain's default network: anatomy, function, and relevance to disease. *Annals of the New York Academy of Sciences*, 1124:1–38, March 2008.

[19] John Graner, Terrence R Oakes, Louis M French, and Gerard Riedy. Functional MRI in the investigation of blast-related traumatic brain injury. *Frontiers in neurology*, 4(March):16, January 2013.

[20] Steen Moeller, Essa Yacoub, Cheryl a Olman, Edward Auerbach, John Strupp, Noam Harel, and Kâmil UÄ§urbil. Multiband multislice GE-EPI at 7 tesla, with 16-fold acceleration using partial parallel imaging with application to high spatial and temporal whole-brain fMRI. *Magnetic resonance in medicine : official journal of the Society of Magnetic Resonance in Medicine / Society of Magnetic Resonance in Medicine*, 63(5):1144–53, May 2010.

[21] Russel A. Poldrack, Jeanette A. Mumford, and Thomas E. Nichols. Modeling brain connectivity. In *Handbook of functional MRI Data Analysis*, pages 130–159. Cambridge University Press, 2011.

[22] Bharat Biswal, F Zerrin Yetkin, Victor M Haughton, and James S Hyde. Functional connectivity in the motor cortex of resting human brain using echo-planar mri. *Magnetic Resonance in Medicine*, 34(4):537–541, 1995.

[23] a Anoop, Pradeep K Singh, Reeba S Jacob, and Samir K Maji. CSF Biomarkers for Alzheimer's Disease Diagnosis. *International journal of Alzheimer's disease*, 2010(Table 1), January 2010.

[24] MSW Esther Heerema. What Is the Alzheimer's Disease Assessment Scale- Cognitive Subscale (ADAS-Cog)?e, 2013.

[25] Matthew Brett, Kalina Christoff, Rhodri Cusack, and Jack Lancaster. Using the talairach atlas with the MNI template. *NeuroImage*, 13(6):85, June 2001.

[26] K J Friston, S Williams, R Howard, R S Frackowiak, and R Turner. Movement-related effects in fMRI time-series. *Magnetic resonance in medicine : official journal of the Society of Magnetic Resonance in Medicine / Society of Magnetic Resonance in Medicine*, 35(3):346–55, March 1996.

[27] Y Behzadi, K Restom, J Liau, and TT Liu. A component based noise correction method (CompCor) for BOLD and perfusion based fMRI. *Neuroimage*, 37(1):90–101, 2007.

[28] Jonathan D Power, Anish Mitra, Timothy O Laumann, Abraham Z Snyder, Bradley L Schlaggar, and Steven E Petersen. Methods to detect, characterize, and remove motion artifact in resting state fMRI. *NeuroImage*, 84:320–41, January 2014.

[29] R Cameron Craddock, G Andrew James, Paul E Holtzheimer, Xiaoping P Hu, and Helen S Mayberg. A whole brain fMRI atlas generated via spatially constrained spectral clustering. *Human brain mapping*, 33(8):1914–28, August 2012.

[30] N Tzourio-Mazoyer, B Landeau, D Papathanassiou, F Crivello, O Etard, N Delcroix, B Mazoyer, and M Joliot. Automated anatomical labeling of activations in SPM using a macroscopic anatomical parcellation of the MNI MRI single-subject brain. *NeuroImage*, 15(1):273–89, January 2002.

[31] Michele Benzi and Christine Klymko. A matrix analysis of different centrality measures. *arXiv preprint arXiv:1312.6722*, 2013.

[32] Ernesto J Sanz-Arigita, Menno M Schoonheim, Jessica S Damoiseaux, Serge a R B Rombouts, Erik Maris, Frederik Barkhof, Philip Scheltens, and Cornelis J Stam. Loss of 'small-world' networks in Alzheimer's disease: graph analysis of FMRI resting-state functional connectivity. *PloS one*, 5(11):e13788, January 2010.

[33] N.F. Rulkov, M.M. Sushchik, L.S. Tsimring, and H.D.I. Abarbanel. Generalized synchronization of chaos in directionally coupled chaotic systems. *Phys. Rev.*, (E 51):980, 1995.

[34] Henk Broer and Floris Takens. Applied mathematical sciences. chapter 6.

[35] Michael G. Rosenblum, Arkady S. Pikovsky, and Jürgen Kurths. Phase Synchronization of Chaotic Oscillators. *Phys. Rev. Lett.*, 76(11):1804—-1807, 1996.

[36] Ed Bullmore and Olaf Sporns. Complex brain networks: graph theoretical analysis of structural and functional systems. *Nature reviews. Neuroscience*, 10(3):186–98, March 2009.

[37] Gabriele Lohmann, Daniel S Margulies, Annette Horstmann, Burkhard Pleger, Joeran Lepsien, Dirk Goldhahn, Haiko Schloegl, Michael Stumvoll, Arno Villringer, and Robert Turner. Eigenvector centrality mapping for analyzing connectivity patterns in fMRI data of the human brain. *PloS one*, 5(4):e10232, January 2010.

[38] Yosef Benjamini, Yoav; Hochberg. Controlling the false discovery rate: a practical and powerful approach to multiple testing. *Journal of the Royal Statistical Society*, 57(1):289–300, 1995.

[39] Zhiqun Wang, Xiuqin Jia, Peipeng Liang, Zhigang Qi, Yanhui Yang, Weidong Zhou, and Kuncheng Li. Changes in thalamus connectivity in mild cognitive impairment: evidence from resting state fMRI. *European journal of radiology*, 81(2):277–85, March 2012.

[40] Yongxia Zhou, John H Dougherty, Karl F Hubner, Bing Bai, Rex L Cannon, and R Kent Hutson. Abnormal connectivity in the posterior cingulate and hippocampus in early Alzheimer's disease and mild cognitive impairment. *Alzheimer's & dementia : the journal of the Alzheimer's Association*, 4(4):265–70, July 2008.

[41] Gaël Chetelat, Béatrice Desgranges, Vincent de la Sayette, Fausto Viader, Karim Berkouk, Brigitte Landeau, Catherine Lalevée, François Le Doze, Benoît Dupuy, Didier Hannequin, Jean-Claude Baron, and Francis Eustache. Dissociating atrophy and hypometabolism impact on episodic memory in mild cognitive impairment. *Brain : a journal of neurology*, 126(Pt 9):1955–67, September 2003.

[42] Kim a Celone, Vince D Calhoun, Bradford C Dickerson, Alireza Atri, Elizabeth F Chua, Saul L Miller, Kristina DePeau, Doreen M Rentz, Dennis J Selkoe, Deborah Blacker, Marilyn S Albert, and Reisa a Sperling. Alterations in memory networks in mild cognitive impairment and Alzheimer's disease: an independent component analysis. *The Journal of neuroscience : the official journal of the Society for Neuroscience*, 26(40):10222–31, October 2006.

[43] Stephen M Smith, Karla L Miller, Gholamreza Salimi-Khorshidi, Matthew Webster, Christian F Beckmann, Thomas E Nichols, Joseph D Ramsey, and Mark W Woolrich. Network modelling methods for FMRI. *NeuroImage*, 54(2):875–91, January 2011.

[44] Cornelis J Stam, Michael Breakspear, Anne-Marie van Cappellen van Walsum, and Bob W van Dijk. Nonlinear synchronization in EEG and whole-head MEG recordings of healthy subjects. *Human brain mapping*, 19(2):63–78, June 2003.